Neurobiology of Disease 184 (2023) 106225

Contents lists available at ScienceDirect

Neurobiology of Disease

journal homepage: www.elsevier.com/locate/ynbdi

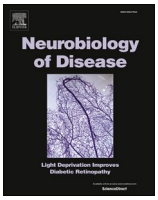

The GRP78-PERK axis contributes to memory and synaptic impairments in Huntington's disease R6/1 mice

Marc Espina [a,b,c,1], Nadia Di Franco [a,b,c,1], Martina Brañas-Navarro [a,b], Irene Rodriguez Navarro [a,b,c], Veronica Brito [a,b,c], Laura Lopez-Molina [a,b,c], Carlos Costas-Insua [c,d,e], Manuel Guzmán [c,d,e], Silvia Ginés [a,b,c,*]

[a] Departament de Biomedicina, Facultat de Medicina, Institut de Neurociències, Universitat de Barcelona, Barcelona 08036, Spain
[b] Institut d'Investigacions Biomèdiques August Pi i Sunyer (IDIBAPS), Barcelona 08036, Spain
[c] Centro de Investigación Biomédica en Red sobre Enfermedades Neurodegenerativas (CIBERNED), Instituto de Salud Carlos III, Madrid 28031, Spain
[d] Instituto Universitario de Investigación Neuroquímica (IUIN), Universidad Complutense, Madrid 28040, Spain
[e] Instituto Ramón y Cajal de Investigación Sanitaria (IRYCIS), Madrid 28034, Spain

ARTICLE INFO

Keywords:
Huntington's disease
hippocampus
ER stress
Memory
PERK
Therapeutics

ABSTRACT

Increasing evidence indicates that a key factor in neurodegenerative diseases is the activation of the unfolded protein response (UPR) caused by an accumulation of misfolded proteins in the endoplasmic reticulum (ER stress). Particularly, in Huntington's disease (HD) mutant huntingtin (mHtt) toxicity involves disruption of the ER-associated degradation pathway and loss of the ER protein homeostasis leading to neuronal dysfunction and degeneration. Besides the role of the UPR in regulating cell survival and death, studies that demonstrate the contribution of sustained UPR activation, particularly of PERK signaling, in memory disturbances and synaptic plasticity deficiencies are emerging. Given the contribution of hippocampal dysfunction to emotional and cognitive deficits seen in HD, we have analyzed the involvement of ER stress in HD memory alterations. We have demonstrated that at early disease stages, ER stress activation manifested as an increase in GRP78 and CHOP is observed in the hippocampus of R6/1 mice. Genetic reduction of GRP78 expression resulted in preventing hippocampal-dependent memory alterations but no motor deficits. Accordingly, hippocampal neuropathology namely, dendritic spine loss and accumulation of mHtt aggregates was ameliorated by GRP78 reduction. To elucidate the signaling pathways, we found that the inactivation of PERK by GSK2606414 restored spatial and recognition memories in R6/1 mice and rescued dendritic spine density in CA1 pyramidal neurons and protein levels of some specific immediate early genes. Our study unveils the critical role of the GRP78/PERK axis in memory impairment in HD mice and suggests the modulation of PERK activation as a novel therapeutic target for HD intervention.

1. Introduction

Neurodegenerative diseases are diverse, and each has unique pathophysiological and clinical hallmarks. However, most share an archetypical pathological attribute: aberrant aggregation of misfolded proteins that eventually triggers endoplasmic reticulum (ER) stress (Aguzzi and O'Connor, 2010; Bertram and Tanzi, 2005; Soto, 2003). In the case of Huntington's disease (HD), the presence of mutant huntingtin (mHtt) toxic oligomers induces the accumulation of misfolded proteins within the ER, thereby triggering the unfolded protein response (UPR) (Duennwald and Lindquist, 2008; Leitman et al., 2013). When activated, the UPR improves protein folding capacity and promotes quality-control mechanisms to ensure adequate proteostasis and cellular health, avoiding abnormal protein aggregation (Hetz and Saxena, 2017). In particular, the master regulatory protein of the UPR is the glucose-regulated protein of 78 kDa (GRP78), also known as BiP or HSP5, whose levels rapidly increase under ER stress load (Casas, 2017). However, in long-term unresolved ER stress, the UPR may induce apoptosis (Hetz and Papa, 2018; Riccardi et al., 2015) by the expression of the transcriptional regulator C/EBP homologous protein (CHOP)

* Corresponding author at: Dept of Biomedical Science, School of Medicine, University of Barcelona, Casanova 143, Barcelona 08036, Spain.
E-mail address: silviagines@ub.edu (S. Ginés).
[1] These authors contributed equally.

https://doi.org/10.1016/j.nbd.2023.106225
Received 24 February 2023; Received in revised form 7 July 2023; Accepted 10 July 2023
Available online 11 July 2023

eventually activating the intrinsic proapoptotic pathway (Tabas and Ron, 2011; Urra et al., 2013).

Sustained UPR activation has been reported in several neurodegenerative diseases including HD (Hetz and Saxena, 2017). Thus, in HD mouse and cellular models as well as in *postmortem* samples from HD patients, ER stress markers such as GRP78, phosphorylated protein kinase RNA-like ER kinase (P-PERK), phosphorylated eukaryotic initiation factor 2α (P-eIF2α), and CHOP are found aberrantly increased and have been directly associated with striatal neurodegeneration (Carnemolla et al., 2009; Duennwald and Lindquist, 2008; Leitman et al., 2014; Leitman et al., 2013; Matthias et al., 2015; Reijonen et al., 2008; Shacham et al., 2019). Notably, recent evidence has reported that chronic and excessive hippocampal ER stress and upregulation of GRP78 expression also play an important role in memory impairment and hippocampal damage (Cai et al., 2015; Cai et al., 2020; Gupta et al., 2021; Keshk et al., 2020; Li et al., 2018; Xu et al., 2019). This might be plausibly mediated by the hyperactivation of the UPR sensor PERK. Accordingly, the reduction of PERK signaling in the hippocampus has been found to enhance neuronal flexibility and improve cognitive function (Sharma et al., 2018; Zhu et al., 2016a). In line with these observations, PERK inhibition has turned out to be beneficial in different pathological settings including Alzheimer's disease (Ma et al., 2013), prion-infected mice (Moreno et al., 2013), frontotemporal dementia (Radford et al., 2015), and traumatic brain injury (Sen et al., 2017; Yan et al., 2017). However, despite all this background, the precise impact of ER stress on memory and synaptic dysfunction in HD, two major neuropathological hallmarks of this neurological disorder (Begeti et al., 2016; Brito et al., 2014; Giralt et al., 2012; Harris et al., 2019; Spires et al., 2004), remains to be addressed.

In this study, we aimed to obtain a detailed and comprehensive picture of how ER stress signaling affects cognition in the R6/1 transgenic HD mouse model. We show that the genetic reduction of GRP78 expression completely prevents spatial and recognition long-term memory deficits in these mice. This was accompanied by a recovery of several pathological hallmarks within the hippocampus, suggesting a detrimental role of the GRP78-mediated ER stress process in HD cognitive symptoms. In line with these data, intraventricular pharmacological inhibition of PERK significantly protected R6/1 mice from cognitive impairment mainly by acting at the synaptic level. Taken together, these findings illustrate the GRP78-PERK axis as an emerging and druggable pathway critically involved in memory loss and synaptic deficits in HD.

2. Materials and methods

2.1. Animals

R6/1 heterozygous transgenic mice expressing a pathogenic fragment of human mutant *Huntingtin* (*mHtt*) exon 1 with CAG repeats ranging from 115 to 150 (Mangiarini et al., 1996) were obtained from The Jackson Laboratory® (Bar Harbor, ME, USA #006471). They were maintained in a BL/6:CBA background together with their non-transgenic wild-type (WT) littermates that served as controls. To study the function of GRP78 we cross-mated R6/1 mice with heterozygous GRP78$^{+/-}$ mice (The Jackson Laboratory® #019549) and generated a new double-mutant R6/1:GRP78$^{+/-}$ mouse line that expresses a pathogenic fragment of human *mHtt* exon 1 and carries a single functional *Grp78* allele. [Note that very early embryonic lethality occurs in *Grp78*$^{-/-}$ mice (Luo et al., 2006)].

Animals used in the experiments were males and females and were housed together in numerical birth order in groups of mixed genotypes. Genotyping was determined by PCR analysis. Animals were housed with access to food and water *ad libitum* in a colony room kept at 19–22 °C and a 40–60% humidity under a 12:12 light/dark cycle. All animal-related procedures were performed in compliance with the National Institutes of Health Guide for the care and use of laboratory animals and were approved by the local animal care committee of the Universitat de Barcelona (448/17) and the Generalitat de Catalunya (9878 P2), following the directive (2010/63/EU) of the European Commission and Spanish (RD53/2013) guidelines for the care and use of laboratory animals.

2.2. Behavioral assessment

Cognitive functions and spontaneous locomotor activity were evaluated in R6/1 and R6/1:Grp78$^{+/-}$ mice at 12–14 weeks of age. Motor learning was assessed by the accelerating rotarod task (ARTP) while spatial and recognition long-term memory was assessed by the novel object location and recognition tasks (NOLT and NORT), respectively. Spontaneous locomotor activity was determined in the Open field test. Protocols were performed as previously described (Brito et al., 2014).

2.3. Novel object location task

Exploration took place in a quadrangular open field (40 × 40 cm sides, 40 cm high). The light intensity was 40 lx throughout the arena, and the room temperature was kept at 19–22 °C, with a humidity of 40–60%. Mice were first habituated to the arena in the absence of objects with spatial cues attached to the walls for 15 min for 2 consecutive days. Spontaneous locomotor activity and time/distance in the periphery/center were measured during this phase. On the third day (NOLT training), 2 identical objects (A and A′) were placed in two adjacent corners of the arena, and mice were allowed to explore for 10 min. 24 h later (NOLT testing), one copy of the familiar object (A) was placed in the same location whereas the other object (A″) was placed in the corner diagonally opposite. In the testing, mice were allowed to explore for 5 min. The arena was rigorously cleaned between animals to avoid odors. Animals were tracked and recorded with SMART® Junior software (Panlab, Spain). Exploration times were recorded and used to calculate the discrimination index as follows:

$$\frac{time\ exploring\ novel\ object - time\ exploring\ familiar\ object}{time\ exploring\ both\ objects} \times 100$$

2.4. Novel object recognition task

Exploration took place following the same standards as indicated before in the NOLT. Mice were first habituated to the arena in the absence of objects for 15 min for 2 consecutive days. Spontaneous locomotor activity and time/distance in the periphery/center were measured during this phase. On the third day (NORT training), mice were allowed to explore two identical objects (B and B′) for 10 min before returning to their home cage. 24 h later (NORT testing), one copy of the familiar object (B) and a new object (C) were placed in the same location as during the training session, and animals were allowed to explore for 5 min. The arena was rigorously cleaned between animals to avoid odors. Animals were tracked and recorded with SMART® Junior software (Panlab, Spain). Exploration times were recorded and used to calculate the Discrimination index as indicated above.

2.5. Accelerating rotarod test

The ARTP was performed as described in (Puigdellívol et al., 2015). Animals were placed on a motorized rod (30-mm diameter, Panlab, Spain), and rotation speed gradually increased from 4 to 40 rpm over the course of 5 min. The fall latency time was recorded when the animal was unable to keep up with the increasing speed and fell. The task was performed four times per day for three consecutive days for a total of 12 trials. Different trials within the same day were separated by 1 h. The results show the average fall latencies per trial during the 3 days of training.

2.6. Open field test

The open field test consisted of a white quadrangular arena (40 × 40 cm sides, 40 cm high) with opaque white walls without external cues. Mice were placed in the center of the arena and were allowed to move freely for 15 min for two consecutive days while being tracked with SMART® Junior software (Panlab, Spain). The arena was rigorously cleaned between trials to eliminate odors. For analysis, spontaneous locomotor activity was measured as the total distance traveled and results show the average distance traveled during the two consecutive days.

2.7. Pharmacological treatment in vivo

2.7.1. Cannula implantation, surgery, and GSK2606414 treatment

WT and R6/1 mice were anesthetized with a mixture of oxygen and isoflurane (4% isoflurane for induction and 2% for maintenance) and small holes were drilled in the skull to target the lateral ventricle at the following coordinates: - 0.22 mm AP, + 1 mm ML, and - 2.4 mm DV. Stainless steel guide cannulas (26-G, Plastics One Inc., Roanoke, VA, USA) were lowered and secured to the skull using surgical screws and acrylic dental cement. Dummy cannulas with the same length to that as the guide cannula were inserted to prevent clogging. One week after surgery, mice were pre-treated with the PERK inhibitor GSK2606414 (MCE®, NJ, USA cat n° HY-18072) (Axten et al., 2012) (20 μM) during 3 alternate days, and then a daily drug administration routine was performed for one week during the behavioral analysis (see the experimental procedure in Fig. 8). GSK2606414 was dissolved in DMSO and further diluted in PBS to a final DMSO concentration of 0.5%. Mice received daily 1 μL of vehicle or 1 μL of 20 μM GSK2606414 using infusion cannulas 0.5 mm longer than guide cannulas. Drugs were infused at 0.5 μL/min in awake and freely moving mice. After infusion, the cannula was left for an additional 3 min to ensure proper diffusion and avoid reflux.

2.7.2. Protein extraction and quantification

Animals were sacrificed by cervical dislocation at different ages. Brains were quickly removed, dissected, frozen in dry ice, and stored at −80 °C until use. Brain tissue was homogenized by sonication in lysis buffer containing 150 mM NaCl, 20 mM Tris-HCl (pH 8.0), 50 mM NaF, 1% NP-40, 10% glycerol supplemented with 1 mM sodium orthovanadate and protease inhibitor mixture (Sigma-Aldrich® cat n° P8340), centrifuged for 15 min at 16.000 g at 4 °C and the supernatants were collected. Protein concentration was determined with a colorimetric assay using the Detergent-Compatible Protein Assay kit (Bio-Rad® cat n° 5,000,116) as indicated in the manufacturer's instructions.

2.7.3. Western Blot analysis

Protein extracts (15-20 μg) were denatured in SDS sample buffer [62.5 mM Tris-HCl (pH = 6.8), 2% (*w/v*) SDS, 10% glycerol, 140 mM ß-mercaptoethanol, and 0.1% (w/v) bromophenol blue)] and boiled at 100 °C for 5 min. They were resolved in 6%–15% polyacrylamide gels (SDS-PAGE) at 30 mA for 1 h. Proteins were then transferred to a nitrocellulose membrane (Amersham® by GE Healthcare Life Sciences®, cat n° 10,600,002) for 1.5 h at 100 V at 4 °C to avoid excessive warming. After 1 h incubation in blocking buffer containing 10% non-fat powdered milk in TBS-T (50 mM Tris-HCl, 150 mM NaCl, pH 7.4, 0.05% Tween 20) membranes were blotted overnight (o/n) at 4 °C with the following primary antibodies: GRP78 (1:1000, Abcam® cat n° ab21685), CHOP (1:1000, Novus Biological® cat n° NBP2–13172), P-PERK(Thr980) (1:1000, ThermoFisher® cat n° MA5–15033), PERK (1:1000, Cell Signaling Technology® cat n° 3192), P-IRE1α(Ser724) (1:1000 Novus Biological® cat n° NB100-2323SS), IRE1α (1:1000 Novus Biological® cat n° NB100-2324SS), ATF6 (1:1000 Novus Biological® cat n° NBP1-40256SS), eIF2α (1:1000 Cell Signaling Technology cat n° 9722), P-eIF2α (Ser51) (1:1000 Cell Signaling Technology cat n° 9721), ATF4 (1:1000 Proteintech® cat n° 10,835–1-AP), XBP1 (1:1000 Novus Biologicals ®cat n°77681ss), P-PSD95(T19) (1:1000, Abcam® cat n° 16,496), PSD95 (1:2000, Cell Signaling Technology® cat n° 34,505), P-CREB(Ser133) (1:1000 Millipore® cat n° 06–519), CREB (1:1000 Cell Signaling Technology® cat n° 9197S), BDNF (1:1000. Icosagen® cat n° 3C11), ARC (1:500 Santa Cruz Technology® cat n° SC-17839), c-FOS (1:1000 Cell Signaling Technology® cat n° 4384), EGR1 (1:1000 Cell Signaling Technology® cat n° 4154S), actin (1:100000, Sigma Aldrich®, cat n° A3854) (the latter at room temperature for 30 min). Membranes were then rinsed three times for 10 min each with TBS-T and incubated for 1 h at room temperature with the appropriate horseradish peroxidase-conjugated mouse or rabbit secondary antibody (1:3000; Promega® cat n° W4021, W4011). After washing for 30 min with TBS-T, membranes were developed using the enhanced chemiluminescence ECL kit (Santa Cruz Biotechnology®, cat n° sc-2048) in a ChemiDoc imaging system (Bio-Rad®). ImageLab® Software Version 6.0 (2017) was used to quantify the different immunoreactive bands relative to the intensity of actin in the same membranes within a linear range of detection for the ECL reagent. Data are expressed as the mean ± SEM of band density.

2.7.4. Tissue fixation and histology

Animals were deeply anesthetized and immediately perfused intracardially with 4% (weight/vol) paraformaldehyde in 0.1 M phosphate buffer. Brains were dissected out and postfixed for 48-72 h shacking at 4 °C in the same solution. Coronal sections (30 μm) of the whole brain were obtained using a vibratome (Leica® VT1000).

2.7.5. Nissl staining and stereology

Nissl staining was performed in floating sections (30 μm in width) separated 240 μm each, after incubation with Cresyl violet solution (0.1 g/L) for 45 min. Then, sections were dehydrated in increasing ethanol concentrations (70% - 100%) and finally mounted with DPX. Bright-field images were acquired at 4× magnification with an AF6000 Leica microscope, and hippocampal volumes were estimated following the Cavalieri method as previously described in (Brito et al., 2014).

2.7.6. Immunoperoxidase staining for mHtt aggregates

For EM48 immunohistochemistry, sections were first incubated for 30 min in 0.01 M sodium citrate buffer (pH 6.0) in a water bath at 80 °C for antigen retrieval. Then, endogenous peroxidases were blocked in PBS containing 5% H_2O_2 for 45 min, and nonspecific protein interactions were also blocked with PBS containing 3% normal horse serum. Tissue was incubated overnight at 4 °C with anti-EM48 (1:500, Merck Millipore®, Billerica, MA, USA, cat n° MAB5374), diluted in PBS containing 0.02% sodium azide and 3% normal horse serum. Sections were then incubated at room temperature for 2 h with a biotinylated anti-mouse antibody (1:200; Pierce; ThermoFisher® Scientific, Waltham, MA, USA, cat n° 32,020), diluted in PBS containing 3% normal horse serum. Sections were washed three times in PBS for 5 min each and incubated for 1.5 h at room temperature in Reagent A (Avidin) and Reagent B (Biotinylated HRP), each of them diluted at 1:56 in PBS, from the ABC kit (Pierce, ThermoFisher® Scientific). The immunohistochemical reaction was developed by incubating the samples for 7 min in diaminobenzidine (DAB), diluted at 1× in PB 0.1 M and 5% H_2O_2. Sections were mounted in gelatinized slides and were left at room temperature to dry completely to finally mount them with DPX. Three coronal hippocampal sections per animal spaced 240 μm apart were chosen for the analysis. Bright-field images from 100% of the CA1 were acquired at 40× magnification with an AF6000 Leica microscope. Automated quantification of the number of nuclear huntingtin aggregates in the CA1 hippocampal region was performed using the Trainable Weka Segmentation Fiji Plugin within the ImageJ® software (a specific pipeline file was created).

2.7.7. Dendritic spine analysis: Golgi-cox staining

Following the manufacturer's instructions, we performed the Golgi-Cox impregnation using the Rapid Golgistain Kit (FD Neurotechnologies®, cat n° PK401). Mice were killed by cervical dislocation at 18–19 weeks of age, brains were quickly removed, and both hemispheres were separated and incubated in a mix of solution A/B for 2 weeks. Then, brains were changed to solution C for 7 days and eventually processed using a cryostat to obtain 100 μm sections mounted in gelatin-coated slides left to dry for 24 h. Sections were stained with the kit's provided solutions and finally, sections were dehydrated and mounted with DPX. We obtained bright field images using a Leica AF6000 epifluorescence microscope with a × 63 numerical aperture objective for dendritic spine analysis. Segments of apical dendrites from hippocampal CA1 pyramidal neurons were selected and spine density was measured manually in the stacks using the ImageJ Plug-in Cell Counter. Spines were marked in the appropriate focal plane preventing double counting and counted in dendritic segments ranging from 20 to 60 μm in length.

2.8. Statistical analysis

All raw data were processed and analyzed using Excel® Microsoft Office and GraphPad Prism® software version 8.0. Results are expressed as the mean ± standard error of the means (SEM). Statistical analysis was performed using the unpaired Student's *t*-Test (two-tailed), one-way or two-way ANOVA followed by the appropriate posthoc tests as indicated in each figure legend. *P* values below 0.05 were considered statistically significant.

3. Results

3.1. GRP78 and CHOP levels are significantly increased in the hippocampus of naïve R6/1 mice

Hippocampal-dependent cognitive alterations are an important neuropathological hallmark in HD (Begeti et al., 2016; Giralt et al., 2012; Harris et al., 2019). Recent evidence has unveiled the contribution of ER stress to synaptic dysfunction and memory deficits in different pathological conditions (Cai et al., 2015; Cai et al., 2020; Gupta et al., 2021; Keshk et al., 2020; Li et al., 2018; Xu et al., 2019). However, no data has been reported on how disruption of ER homeostasis may affect HD hippocampal function. Therefore, we first analyzed the ER stress response in the hippocampus, striatum, and cerebral cortex of R6/1 male mice at different disease stages (12 weeks, 16 weeks and 20 weeks, corresponding to pre-symptomatic, early symptomatic and late symptomatic stages). We measured the levels of GRP78 as the main chaperone acting as an ER stress sensor (Casas, 2017; Wang et al., 2009) and CHOP as a key UPR pro-apoptotic factor (Cai et al., 2015; Tabas and Ron, 2011; Urra et al., 2013). We found increased GRP78 and CHOP protein levels in the hippocampus of R6/1 mice compared to WT mice at different disease stages (Fig. 1A and 2A). No changes between genotypes were detected for GRP78 and CHOP within the striatum at early disease stages (Fig. 1B and 2B) while a slight, but significant decrease for cortical GRP78 levels was observed (Fig. 1C and 2C). Interestingly, at late stages, GRP78 was found to be significantly increased in the striatum of R6/1 mice while only a tendency was observed in the cortex. Similar results were detected for CHOP at 20 weeks of age. In view of these data, similar studies were performed in the hippocampus of female mice. Significantly higher levels of GRP78, starting at 16 weeks of age, were found in R6/1 mice compared to WT mice. In contrast, CHOP levels were found increased only at 20 weeks of age, suggesting a delay of the ER stress response in R6/1 female compared to R6/1 males. Next, and taking advantage of published RNA-seq data generated from different HD mice and tissues (Langfelder et al., 2016 and Lee et al., 2020) we integrated our protein results on GRP78 and CHOP with published datasets of RNA expression (Supplementary Table 1). Overall, modest changes have been found in the mRNA expression of some ER stress markers in the striatum and cortex of HD mice, particularly in those with higher CAG number (Q140, Q175 and R6/2 mice) and at late stages of the disease (6 months for KI mice and 9 weeks for R6/2) with no significant changes in the hippocampus of Q175 mice.

Next, and given the role of CHOP as a transcription factor we next explored whether genes known to be differentially explored in the hippocampus of HD mice were downstream targets of CHOP (Supplementary Fig. 2). We integrated published data of hippocampal differential expressed genes between zQ175 and WT mice (Langfelder et al., 2016) with genes directly regulated by CHOP in response to stress (Han et al., 2013). When comparing all the differential expressed genes observed in zQ175 mice with genes directly regulated by CHOP in response to ER stress, we identified only 1.2% of overlapping genes, while 21% and 78% of the differential expressed genes were unique for each condition suggesting a modest contribution of CHOP transcriptional activity to hippocampal stress gene dysregulation.

Altogether, these results demonstrate an early ER stress in the hippocampus of R6/1 mice.

3.2. PERK signaling pathway is preferentially induced in the hippocampus of naïve R6/1 mice

To further characterize the ER stress response in the hippocampus of R6/1 mice, we next determined the activation of the three major UPR sensor proteins, namely: PERK, ATF6, and IRE1α. PERK and IRE1α activation were evaluated by measuring its phosphorylation at Thr980 and Ser724 respectively (Hetz et al., 2015; Walter and Ron, 2011), while ATF6 activity was assessed by measuring its proteolytic cleavage (Fernandez-Fernandez et al., 2011). Total hippocampal lysates from R6/1 and WT mice at the age of 12 weeks were analyzed. As shown in Fig. 3A, a significant increase in P-PERK levels was found in R6/1 mice compared to age-matched WT mice. In contrast, P-IRE1α and ATF6 levels (full-length and cleaved forms) remained unaltered (Fig. 3B and C). Next, P-eIF2α, ATF4 and active spliced XBP1 (XBP1s) were evaluated as downstream effectors of the UPR sensor proteins. No major changes were observed neither for eIF2α phosphorylation nor ATF4 levels (Fig. 3D and Fig. 3E). However, a slight but significant decrease in XBP1s was found in R6/1 compared to WT mice (Fig. 3F).

These results suggest that activation of the GRP78/PERK axis is associated with the ER stress response in the hippocampus of R6/1 mice at early disease stages.

3.3. Memory deficits but not motor performance alterations can be prevented by genetic reduction of GRP78 expression in R6/1 mice

To explore how increased hippocampal ER stress response may contribute to HD memory disturbances, a new double-mutant (R6/1: GRP78$^{+/-}$) mice with reduced levels of GRP78 expression was generated by cross-mating R6/1 mice with heterozygous GRP78$^{+/-}$ mice (Luo et al., 2006). GRP78 levels were found significantly decrease in hippocampal lysates from double-mutant mice compared to either R6/1 or WT mice while a normalization to WT levels was found for CHOP expression (Fig. 4A). No gross changes were noticed when GRP78 and CHOP protein levels were analyzed in striatal and cortical extracts from double-mutant mice (Fig. 4B and C). Based on these results and given the increase in PERK activation observed in the hippocampus of R6/1 mice, we next evaluated the effect of GRP78 reduction in PERK activation. Similar to data found for CHOP expression, double-mutant mice exhibited comparable P-PERK levels to WT or heterozygous GRP78$^{+/-}$ mice. These results reveal that genetic reduction of GRP78 expression in R6/1 mice normalizes hippocampal levels of CHOP and P-PERK ameliorating the sustained ER stress response.

Next, long-term spatial and recognition memories were evaluated in double-mutant mice by the Novel Object Location and Novel Object Recognition Tasks (NOLT and NORT, respectively) (Fig. 5). During the

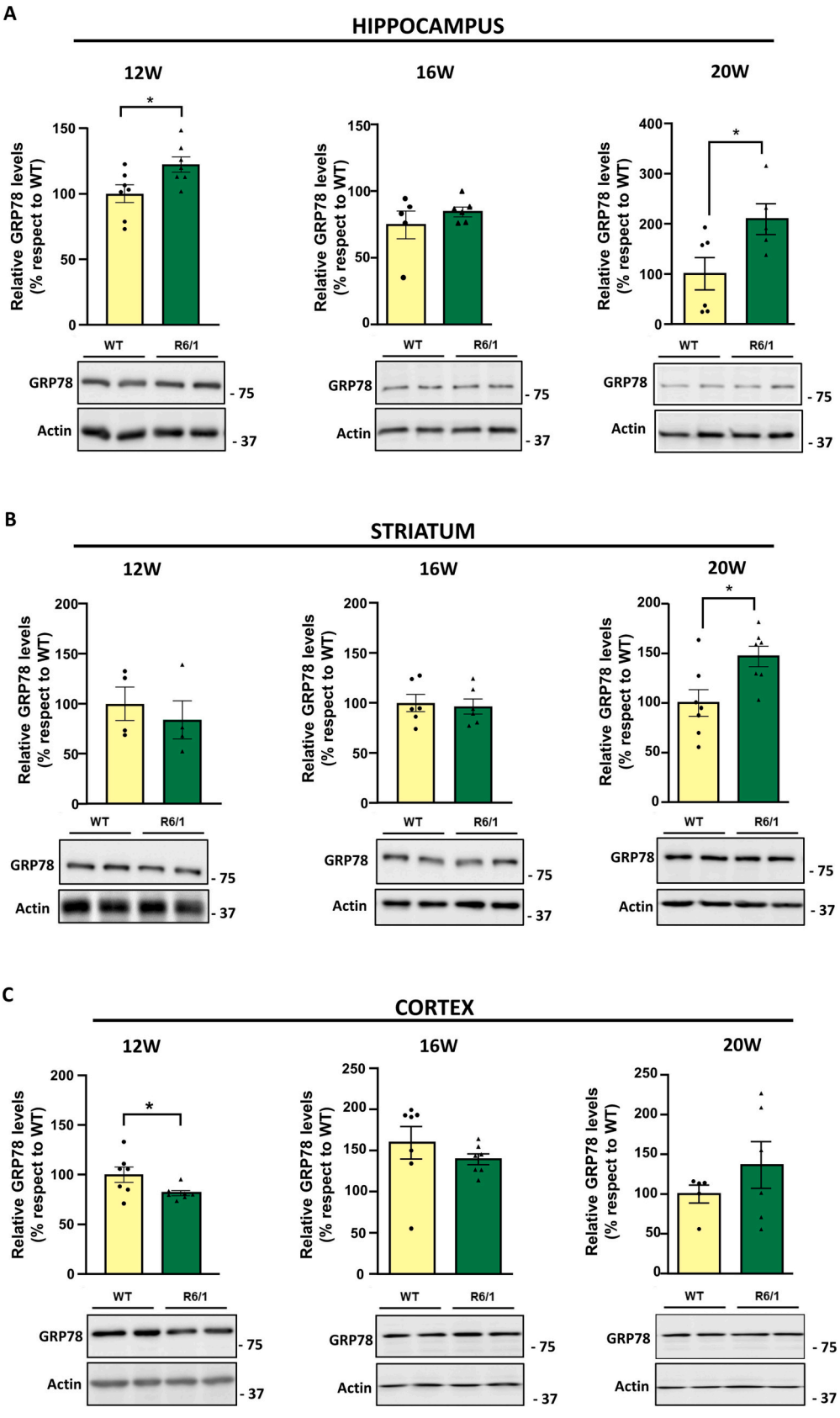

Fig. 1. GRP78 levels are increased in the hippocampus of R6/1 mice. Representative immunoblots showing the levels of GRP78 in total lysates from A hippocampal, B striatal, and C cortical extracts of WT and R6/1 male mice at different disease stages (W, weeks; $n = 6$–7 mice/group). Actin was used as a loading control. Histograms show protein levels relative to actin and expressed as percentage of WT mice. Data represent mean ± SEM. *$P < 0.05$ *vs* WT mice determined by unpaired Student's *t*-test.

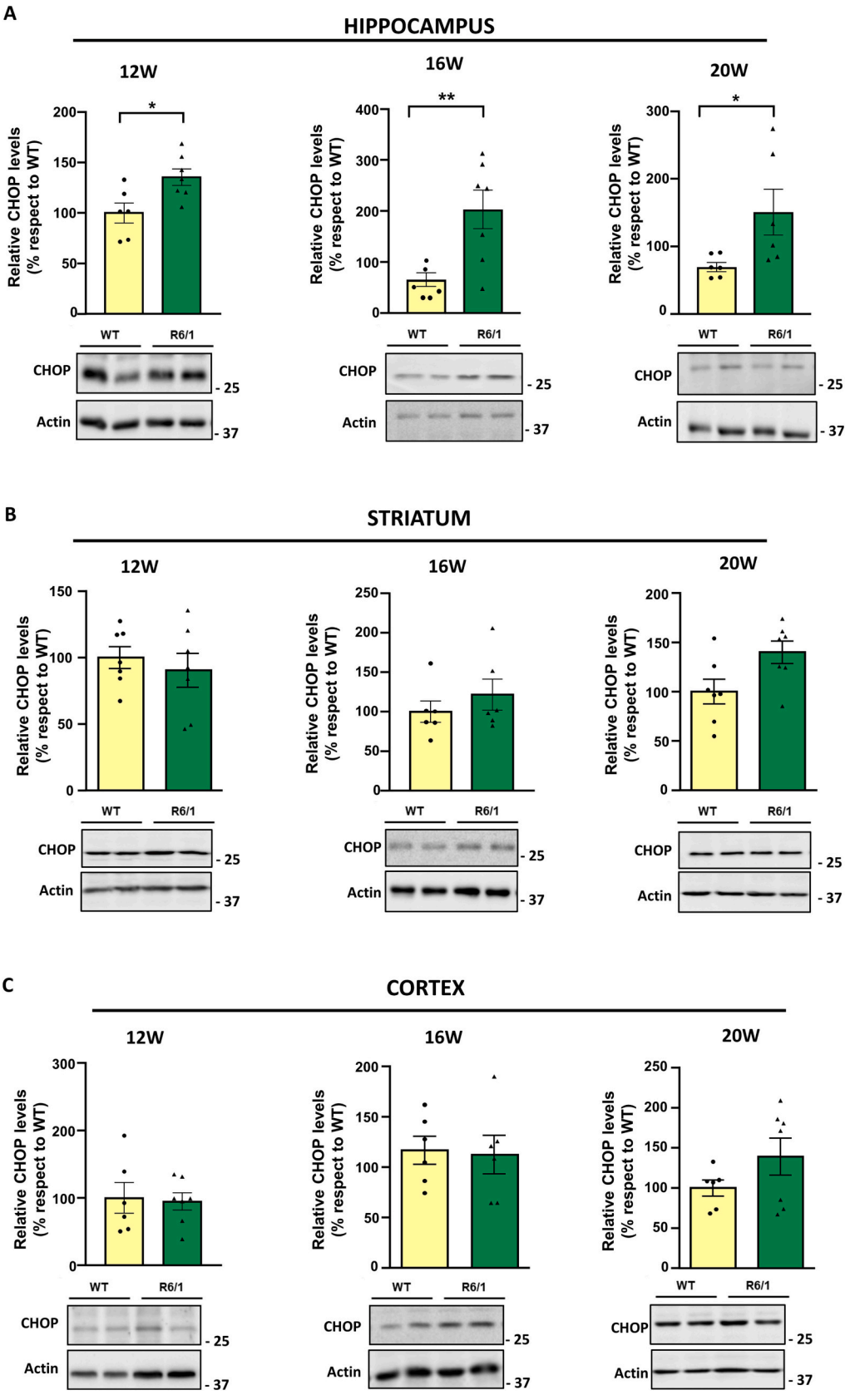

Fig. 2. CHOP levels are increased in the hippocampus of R6/1 mice. Representative immunoblots showing the levels of CHOP in total lysates from A hippocampal, B striatal, and C cortical extracts of WT and R6/1 male mice at different disease stages (W, weeks; n = 6–7 mice/group). Actin was used as a loading control. Histograms show protein levels relative to actin and expressed as percentage of WT mice. Data represent mean ± SEM. *P < 0.05, **P < 0.01 *vs* WT mice determined by unpaired Student's *t*-test.

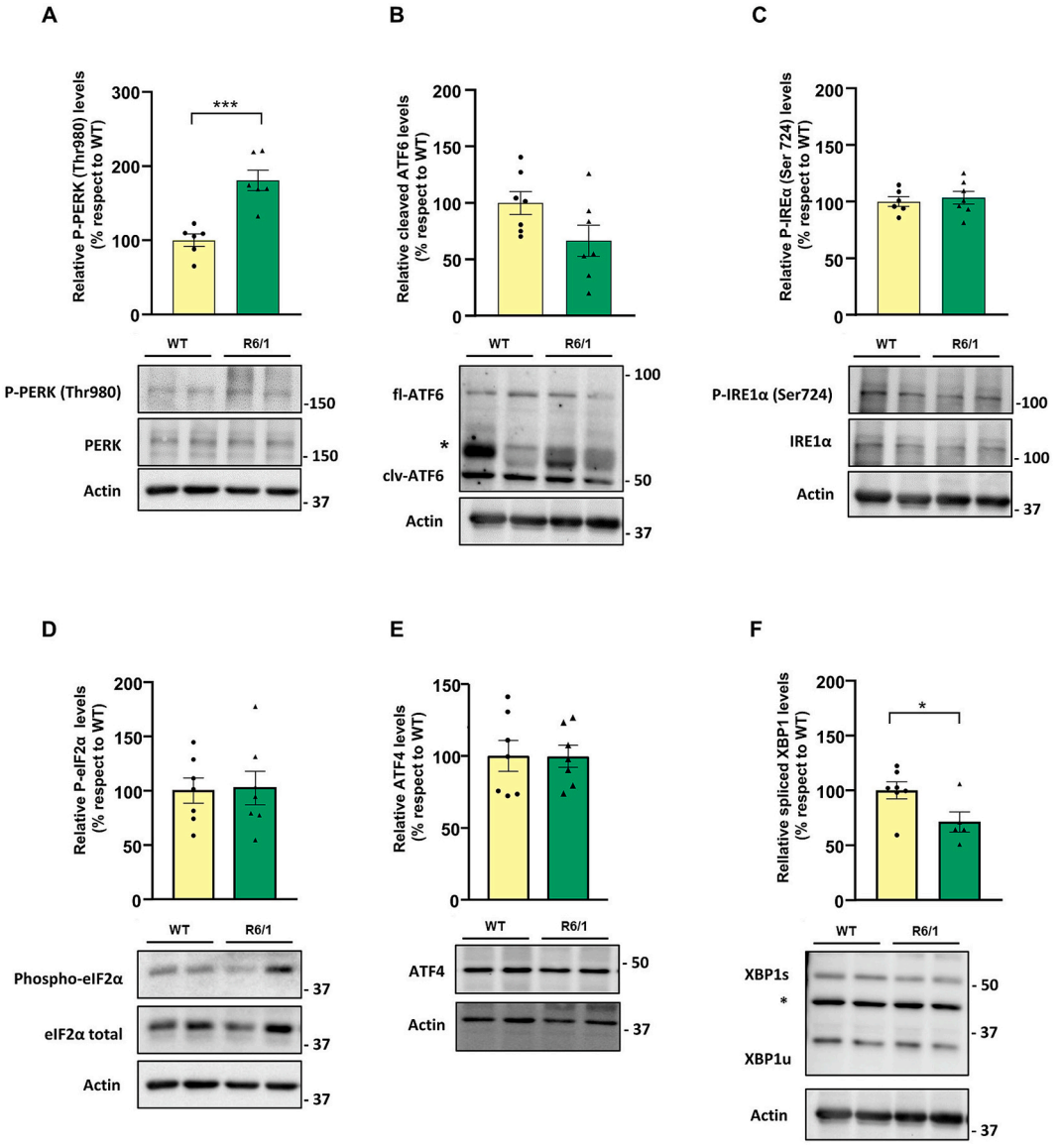

Fig. 3. Selective induction of PERK in the hippocampus of young R6/1 mice. Representative immunoblots showing the levels of P-PERK (Thr980) and PERK (A), fl-ATF6 (full-length) and clv-ATF6 (cleaved) (B), P-IRE1α (Ser724) and IRE1α (C) in total lysates from hippocampal extracts of WT and R6/1 male mice at 12 weeks of age. (*) indicates an unspecific band recognized by the ATF6 antibody. Actin was used as a loading control. Histograms show protein levels relative to actin and expressed as percentage of WT mice. Data represent the mean ± SEM (W, weeks; n = 6–7 mice/group). ***$P < 0.001$ *vs* WT mice determined by unpaired Student's *t*-test. Representative immunoblots showing the levels of P-eIF2α (Ser 51) and eIF2α (D), ATF4 (E), XBP1s (spliced form) and XBP1u (unspliced form) (F) in total lysates from hippocampal extracts of WT and R6/1 male mice at 12 weeks of age. (*) indicates an unspecific band recognized by the XBP1 antibody. Actin was used as a loading control. Histograms show protein levels relative to actin and expressed as percentage of WT mice. Data represent the mean ± SEM (W, weeks; n = 6–7 mice/group). *$P < 0.05$ *vs* WT mice determined by unpaired Student's *t*-test.

training sessions, all mice were presented with two similar objects (A and A') that were explored equally showing no preference for either location or object (Fig. 5B and C). 24 h later, when long-term memory was assessed, R6/1 mice were not able to discriminate the new location **(NOLT;** Fig. 5B**)** nor the novel object **(NORT** Fig. 5C**)** from the familiar ones. Notably, double-mutant mice exhibited preserved spatial and recognition memories with a similar percentage of time exploring the new location as well as discrimination indexes comparable to WT mice. Then, motor performance was evaluated by the accelerating rotarod task (motor learning) and the open field test (motor coordination). As shown in Fig. 6, R6/1 and double-mutant mice showed poor motor learning ability, manifested as reduced latency to fall over trials compared to either WT or GRP78$^{+/-}$ mice (Fig. 6A). When the spontaneous locomotor activity was assessed in the open field test, once again, both R6/1 and double-mutant mice traveled less distance in the arena over the course of 15 min compared to WT or GRP78$^{+/-}$ mice (Fig. 6B). To exclude anxiety-like behaviors due to the reduction of GRP78 expression, the percentage of time spent in the periphery *versus* the center of the open-field arena was calculated and no significant differences were found between genotypes (Fig. 6B). These data suggest that the reduction of GRP78 expression in R6/1 mice ameliorates ER stress in the hippocampus and prevents hippocampal-dependent long-term memory deficits but not motor impairments.

3.4. Dendritic spine loss in CA1 pyramidal neurons can be prevented by genetic reduction of GRP78 expression in R6/1 mice

Our previous data demonstrate that reduction of GRP78 expression in R6/1 mice prevents memory deficits but not motor disturbances, pointing to a regional effect of ER stress activation at early HD stages.

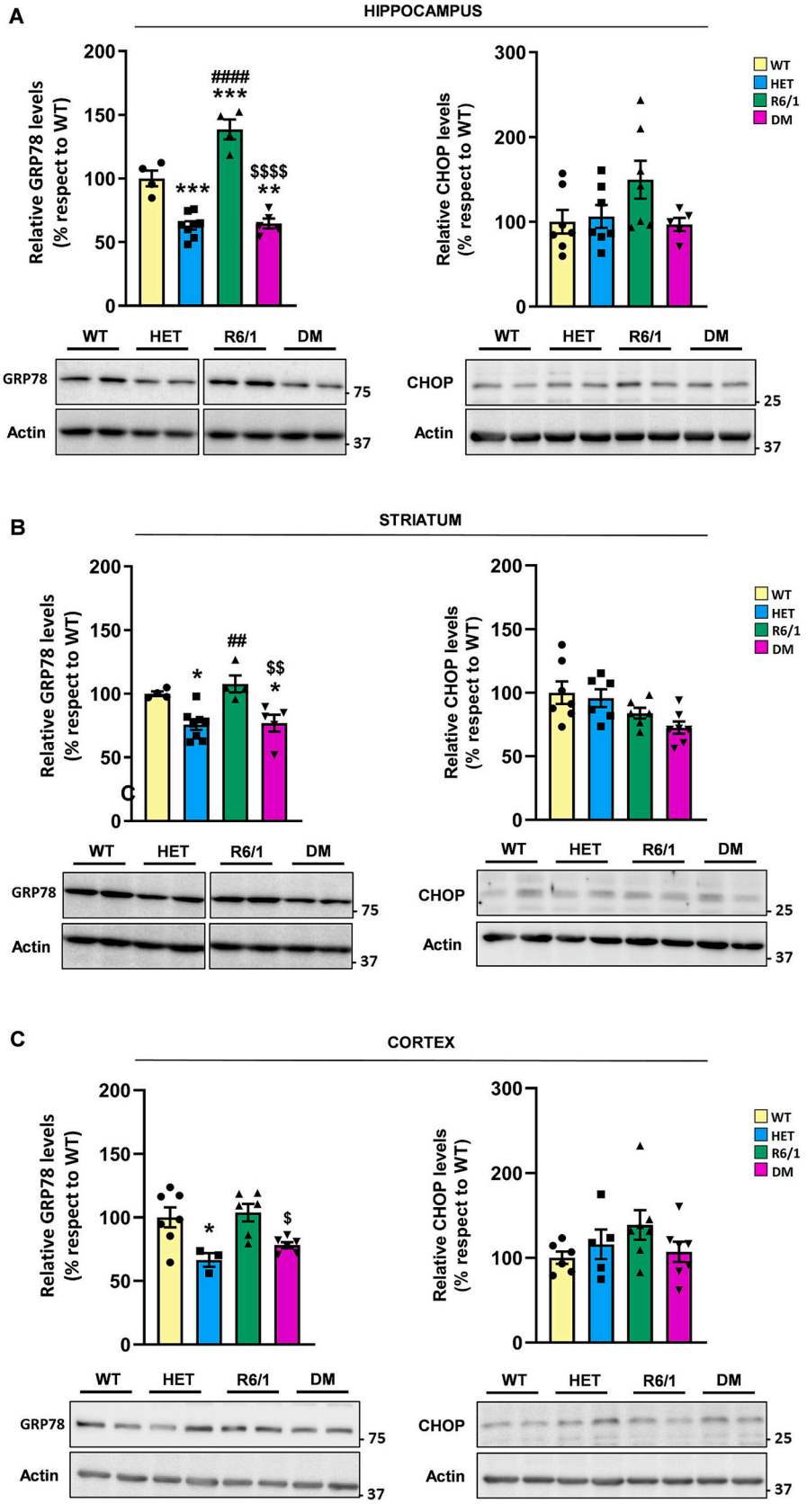

Fig. 4. Genetic reduction of GRP78 expression normalizes hippocampal CHOP levels in R6/1 mice. Representative immunoblots showing the levels of GRP78 and CHOP in total lysates from A hippocampal, B striatal, and C cortical extracts of WT, heterozygous GRP78$^{+/-}$ (HET), R6/1 and double-mutant R6/1: GRP78$^{+/-}$ (DM) male mice at 12 weeks of age. Actin was used as a loading control. Histograms show protein levels relative to actin and expressed as percentage of WT mice. Data represent the mean ± SEM (W, weeks; *n* = 4–7 mice/group). *P < 0.05, **P < 0.01, ***P < 0.001 *vs* WT mice. ##P < 0.01, ####P < 0.0001 *vs* HET mice. $P < 0.05, $$P < 0.01, $$$$P < 0.0001 *vs* R6/1 mice. All data were analyzed by One-way ANOVA followed by Tukey's test.

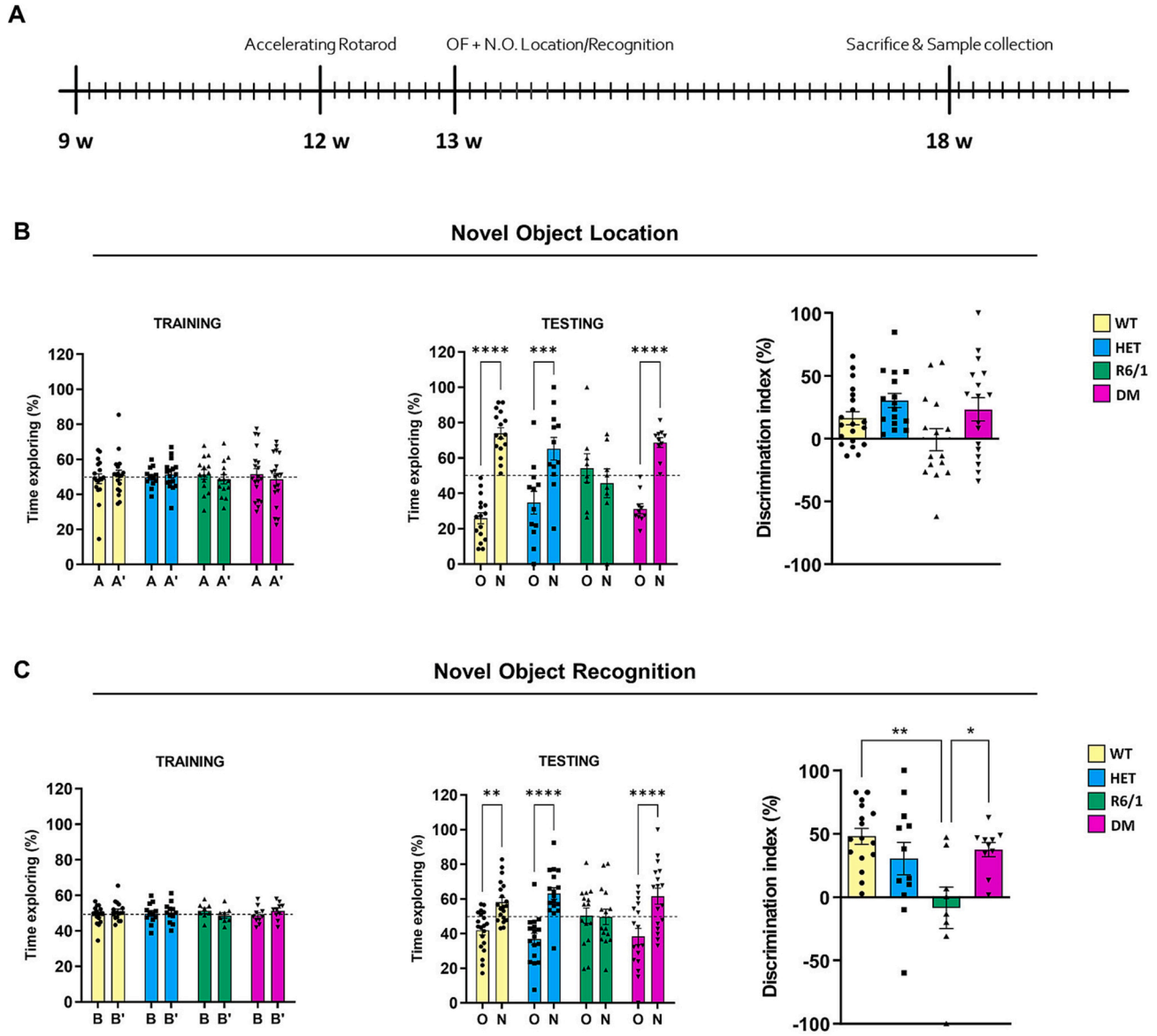

Fig. 5. Genetic reduction of GRP78 expression prevents spatial and recognition memory deficits in R6/1 mice. A Timeline representing experimental behavioral design. Performance in spatial B (NOLT) and recognition C (NORT) memory tests. Left: Exploration time during training and testing sessions expressed as a percentage (%). The dashed line marks the chance level of exploration. Data were analyzed by Two-way ANOVA followed by Sídák's test. **P < 0.01, ***P < 0.001, ****P < 0.0001 compared to the percentage of time exploring the familiar object. Right: Discrimination indexes are expressed as a percentage (%). Data were analyzed by One-way ANOVA followed by Tukey's test. *P < 0.05, **P < 0.01. All data represent the mean ± SEM (n = 16–20 mice/group).

Therefore, we next focused our analysis on hippocampal neuropathology. First, a quantitative stereological analysis of the hippocampus volume was performed (Fig. 7A). No significant differences were found between genotypes suggesting no gross anatomical alterations either in R6/1 or double-mutant mice. Next, structural synaptic plasticity was assessed by measuring apical dendritic spine density in CA1 pyramidal neurons (Fig. 7B). R6/1 mice showed a significant decrease in spine density compared to WT mice, a decrease that was prevented in double-mutant mice. These data suggest that the hippocampal-dependent cognitive improvements observed in double-mutant mice might be related to a recovery of structural synaptic plasticity.

3.5. Hippocampal intranuclear mHtt inclusions can be reduced by genetic reduction of GRP78 expression in R6/1 mice

Another neuropathological hallmark of HD is the aggregation of mHtt in neuronal intranuclear inclusions (Bates, 2003; DiFiglia et al., 1997; Vonsattel et al., 1985). Therefore, we evaluated whether the reduction of GRP78 expression in R6/1 mice also ameliorates the formation of mHtt inclusions. Immunohistochemical analysis of EM48 antibody staining was performed in coronal hippocampal slices from R6/1 and double-mutant mice. As previously described by our group and others (Anglada-Huguet et al., 2014; García-Forn et al., 2018) EM48-positive intranuclear inclusions were found in the hippocampal CA1 region of R6/1 mice (Fig. 8). Remarkably, GRP78 expression reduction in double-mutant mice induced a significant decrease in intranuclear mHtt inclusion density suggesting that amelioration of ER stress in R6/1 mice contributes to delaying the onset of hippocampal neuropathology and long-term memory deficits.

3.6. Pharmacological PERK inhibition prevents long-term memory deficits in R6/1 mice

Given the observed beneficial effects of reducing GRP78 expression

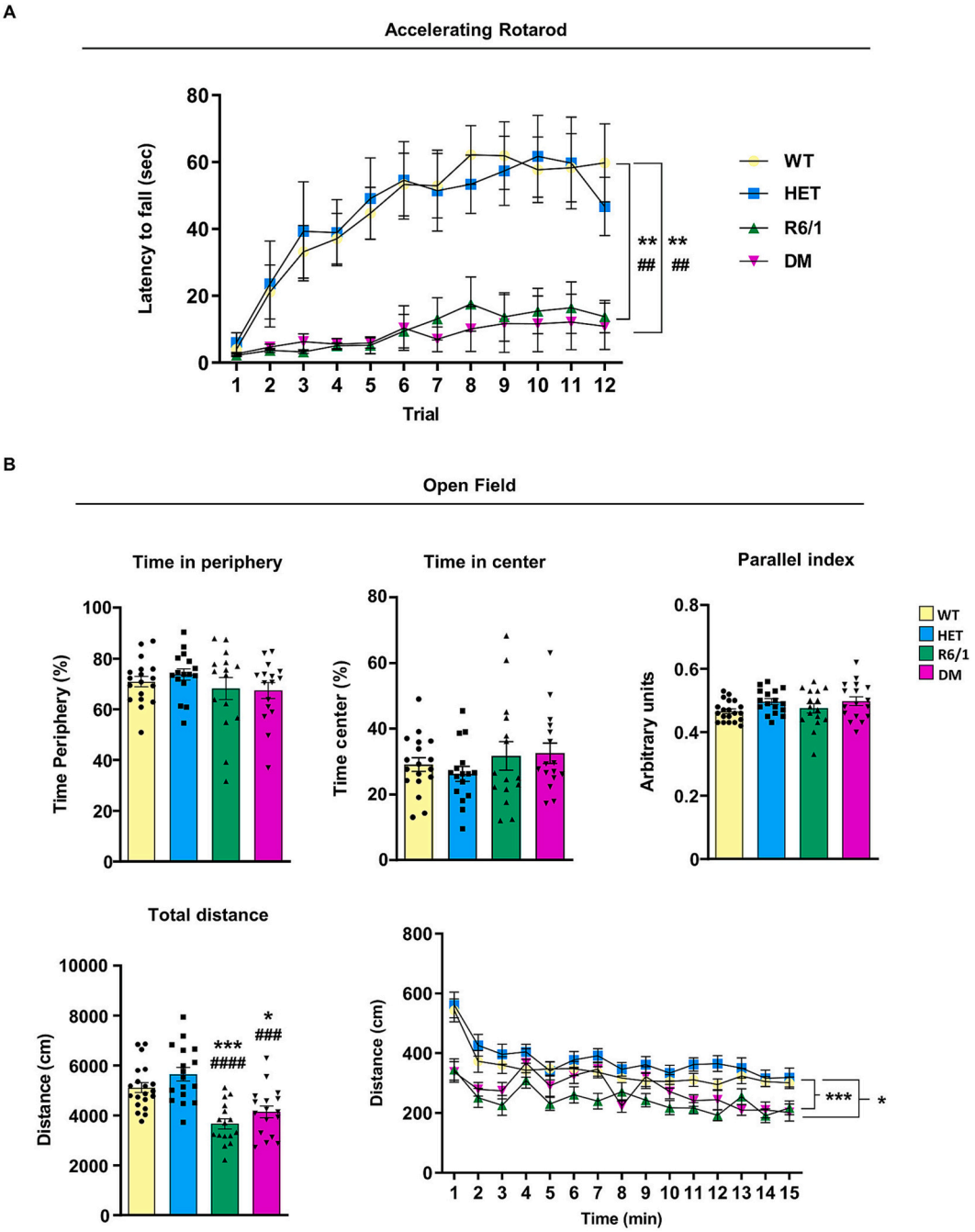

Fig. 6. Genetic reduction of GRP78 expression does not prevent motor impairments in R6/1 mice. A Latency to fall in the accelerating rotarod task at 12–13 weeks of age. Data were analyzed by Two-way ANOVA followed by Tukey's test. **P < 0.01 *vs* WT, ##P < 0.01 *vs* HET. All data represent the mean ± SEM (n = 18–20 mice/group). B Anxiety-like behavior was measured by time spent in the periphery/center of the open field arena. Spontaneous locomotor behavior was analyzed by measuring the total distance traveled and the parallel index. Data were analyzed by One-way ANOVA followed by Tukey's test. *P < 0.05, ***P < 0.001 *vs* WT mice. ###P < 0.001, ####P < 0.0001 *vs* HET mice. All data represent the mean ± SEM (n = 12–15 mice/group).

on hippocampal neuropathology and memory deficits in R6/1 mice and recent evidence suggesting that activation of PERK may lead to cognitive impairments (Shacham et al., 2021), we next asked whether PERK inhibition could influence memory impairments in R6/1 mice. To this aim, the PERK inhibitor GSK2606414 (1 μl volume, 20 μM) was infused intraventricularly on 3 alternate days before the cognitive evaluation period, and then daily during the behavioral assessment (Fig. 9A). First, we evaluated the effect of GSK2606414 on PERK phosphorylation levels by Western blot. We observed a significant treatment effect on P-PERK levels with decreased phosphorylation both in WT and R6/1 mice (Fig. 9B). Since the role of PERK in hippocampal-dependent memory has been associated with the activation of eIF2α (Ma et al., 2013; Moreno et al., 2012), we next analyzed phosphorylation of eIF2α at Ser51 in vehicle and GSK2606414-treated R6/1 mice (Fig. 9B). Surprisingly, no significant changes were detected in P-eIF2α neither between genotypes nor between treatments, suggesting that the PERK/eIF2α axis is not involved in R6/1 memory disturbances. Next, the effect of PERK inhibition was evaluated on long-term spatial and recognition memory by the NOLT and NORT tasks (Fig. 9C). A similar percentage of time exploring both the novel location and object was found in treated-R6/1 mice compared to vehicle-treated WT mice. Notably and in line with the critical role of PERK in cognitive functions (Sharma et al., 2018; Zhu

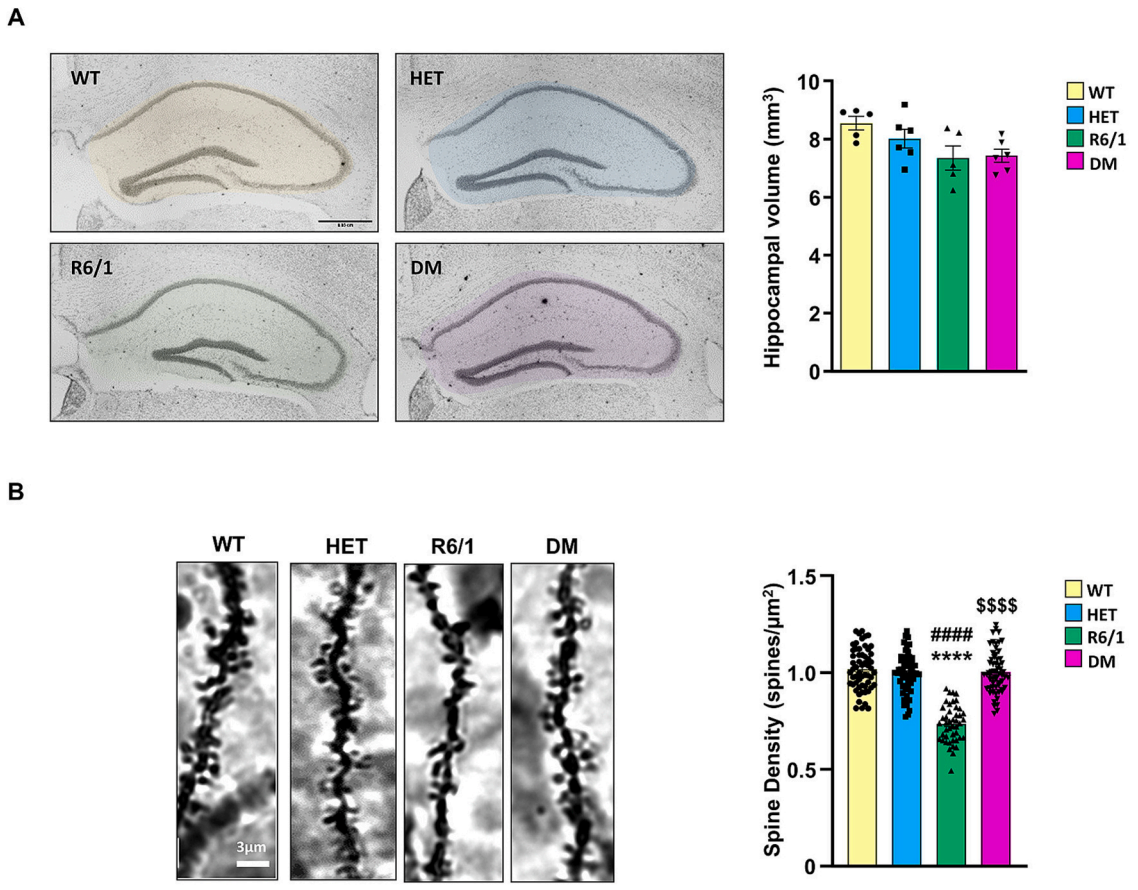

Fig. 7. Genetic reduction of GRP78 counteracts dendritic spine pathology of CA1 pyramidal neurons in R6/1 mice. A Hippocampal volumes of Nissl-stained coronal sections were stereologically quantified in WT, heterozygous GRP78$^{+/-}$ (HET), R6/1 and double-mutant R6/1:GRP78$^{+/-}$ (DM) mice at the age of 18 weeks. Data were analyzed by One-way ANOVA followed by Tukey's Test. All data represent the mean ± SEM (n = 5–6 mice/group). B Representative photomicrographs showing apical dendrites from CA1 pyramidal neurons from WT, heterozygous GRP78$^{+/-}$ (HET), R6/1, and double-mutant R6/1:GRP78$^{+/-}$ (DM) mice at the age of 18 weeks of age. Scale bar 3 µm. The histogram shows a quantitative analysis of dendritic spine density per micrometer of dendritic length. Data were analyzed by One-way ANOVA followed by Tukey's Test. ****P < 0.0001 *vs* WT, $$$$ P < 0.0001 *vs* R6/1, #### P < 0.0001 *vs* HET. All data represent the mean ± SEM (>50 dendrites/group: n = 4 mice/group).

et al., 2016a), GSK2606414-treated WT mice are impaired in spatial and recognition memory tasks. These data point to an important contribution of hippocampal ER stress to spatial and recognition memory deficits in R6/1 mice through the activation of PERK.

3.7. Pharmacological PERK inhibition ameliorates dendritic spine loss and reduction of memory-related gene expression in R6/1 mice

Our previous results suggest that treatment with GSK2606414 prevents memory decline in R6/1 mice independently of eIF2α phosphorylation. Therefore, we were interested in defining other molecular mechanisms by which the inactivation of PERK could be exerting its beneficial effects. Our previous data revealed that the reduction of GRP78 expression had a positive impact on hippocampal structural synaptic plasticity. Thus, we next evaluated whether the pharmacological inhibition of PERK could induce a similar effect. Interestingly, we found that GSK2606414 treatment ameliorated the loss of apical dendritic spine density in pyramidal CA1 neurons in R6/1 mice while reducing the number of spines in treated-WT mice (Fig. 10) suggesting that the GRP78/PERK axis is involved in HD hippocampal structural synaptic alterations and, therefore, in cognitive deficits.

Next, the expression of some synaptic-related proteins and memory-related genes were evaluated in the hippocampus of vehicle and treated-R6/1 mice. Given that phosphorylation of PSD95 by PERK at T19 residue has been reported to negatively affect the stability of dendritic spines (Sen et al., 2017), we first analyzed the levels of total and P-PSD95 in hippocampal extracts. No significant changes were found between genotypes and treatments in WT nor R6/1 mice, suggesting that this pathway is not involved in the observed HD cognitive deficits (Fig. 11A). Then, CREB and BDNF, two important proteins critical for synaptic function and memory formation were analyzed (Giralt et al., 2013; Puigdellívol et al., 2016). Again, no differences were found when comparing genotypes and treatments (Fig. 11B and C). Finally, we analyzed the levels of some immediate early genes known to be activated by neuronal activity and regulate memory and synaptic plasticity (Herdegen and Leah, 1998; Korb and Finkbeiner, 2011; Minatohara et al., 2016). A positive effect of PERK inhibition was observed in R6/1 mice, showing an increase in both Arc and c-Fos protein levels compared to vehicle-treated mice (Fig. 11D and E). In contrast, inhibition of PERK was not able to rescue the significant decrease in Egr1 protein levels observed in R6/1 mice compared to WT mice (Fig. 11<F). Therefore, pharmacological inhibition of PERK increases the protein levels of Arc and c-Fos with no changes in Egr1. Altogether, these data suggest that inhibition of PERK positively affects memory function in HD by acting on structural and synaptic plasticity.

4. Discussion

ER stress, a common pathological hallmark of several neurodegenerative diseases including HD, elicits the activation of the UPR signaling cascade to ensure correct proteostasis and cellular health (Hetz and Saxena, 2017; Riccardi et al., 2015). Specifically, in HD it has been

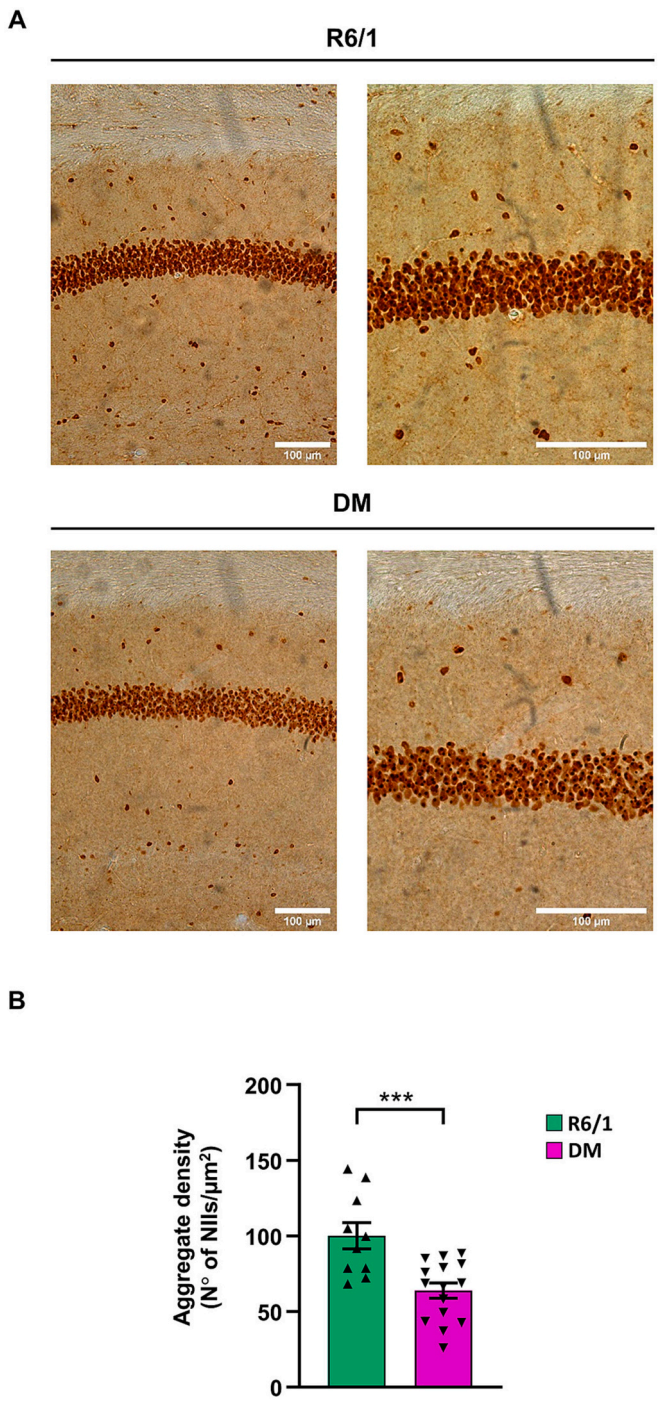

Fig. 8. Genetic reduction of GRP78 decreases mHtt aggregates in the hippocampus of R6/1 mice. A Representative photomicrographs showing nuclear EM48 immunostaining in the hippocampal CA1 region of R6/1 and double-mutant R6/1:GRP78$^{+/-}$ (DM) mice at the age of 18 weeks. Scale bar 100 µm. B Histogram represents the density of EM48-positive neuronal intranuclear inclusions (NIIs). Each symbol represents the mean density of aggregates from one CA1 hemisphere. ***P < 0.001 *vs* R6/1 mice by Student's *t*-Test. Data represent the mean ± SEM (All CA1 NIIs were quantified in each hemisphere from n = 5–6 mice/group).

reported that mHtt might cause ER stress by sequestering and depleting the cytosolic chaperone p97/VCP and its cofactors Npl4 and Ufd1, both essential for the ERAD pathway enhancing protein accumulation in the ER (Duennwald and Lindquist, 2008; Leitman et al., 2013). The resultant ER stress causes chronic upregulation of UPR markers which were observed in HD cellular and animal models and in *postmortem* samples from HD patients (Carnemolla et al., 2009; Duennwald and Lindquist, 2008; Leitman et al., 2014; Leitman et al., 2013; Reijonen et al., 2008; Shacham et al., 2019). However, most of these studies have been focused on the association between ER stress and striatal cell death or dysfunction with no studies addressing the possible link between HD memory impairment and ER stress. Indeed, defects in memory function following induction of ER stress have been previously reported in the context of AD and recent evidence has underlined the importance of ER stress in synaptic function and memory formation under healthy conditions (Lin et al., 2018; Sen, 2019).

Here, we have defined the contribution of the GRP78/PERK axis, a major transducer of ER stress signaling, to HD hippocampal neuropathology and memory dysfunction. We show that early in the disease process, in stages prior to motor coordination deficits (Mangiarini et al., 1996) a sustained ER stress activation, manifested by increased protein levels of GRP78, CHOP and P-PERK is observed in the hippocampus. Remarkably, any significant alteration in GRP78 and CHOP protein levels was found in the striatum or the cortex of R6/1 mice at early disease stages. These results are in accordance with previous studies showing no significant alterations in GRP78 protein expression in the striatum of symptomatic R6/1 mice (Fernandez-Fernandez et al., 2011) or GRP78 and CHOP protein levels in Knock-in$^{Q111/Q111}$ striatal cells following ER stress induction by tunicamycin (Leitman et al., 2014). Similarly, previous published data from RNA-seq data generated from different HD mice and tissues revealed modest RNA changes in the mRNA expression of some ER stress markers in the striatum and cortex of HD mice, particularly in those with higher CAG number (Q140, Q175 and R6/2) and at late stages of the disease (6 months and 9 weeks). Indeed, at very late disease stages we also found in R6/1 mice a significant increase for GRP78 in the striatum while a tendency in the cortex. Actually, other HD mouse models (YAC128 at 18 months of age mice and R6/2 mice at 13 weeks of age) exhibited increased levels of GRP78 and CHOP in the striatum and cortex (Lee et al., 2012) which, may indicate that the ER stress response propagates in a specific brain region manner along HD disease progression, showing the striatum and cortex a late ER stress response.

Since previous studies have suggested that neuronal excitability can induce ER stress response (Liu et al., 2019; Liu et al., 2021), protein levels of both GRP78 and CHOP were also investigated in behavioral trained mice. A similar increase in GRP78 and CHOP was detected in R6/1 compared to WT animals suggesting that neuronal activity does not differentially affect ER stress response in R6/1 mice (data not shown).

To investigate the specific contribution of GRP78 to early memory disturbances in HD, we generated a new double-mutant mouse by crossbreeding R6/1 mice with heterozygous GRP78$^{+/-}$ mice. Preserved spatial and recognition memories were found in these double-mutant mice suggesting that ER stress activation in the HD hippocampus negatively affects cognitive function. In accordance to these results, in ApoE4 transgenic mice used as a model of AD, the reduction of GRP78 levels by curcumin treatment improved spatial memory deficits in the Morris water maze test (Kou et al., 2021). Likewise, cognitive impairment in rats induced by microcystin-LR was prevented by treatment with the ER stress blocker tauroursodeoxycholic acid (TUDCA) along with a reduction in the ER stress response (Cai et al., 2015). Notably, TUDCA treatment also prevented spine density loss and synaptic activity dysfunction in APP/PS1 mice (Ramalho et al., 2013) suggesting that the detrimental effect of ER stress on hippocampal function is related to changes in structural plasticity. In line with this hypothesis, our results have revealed that the reduction of GRP78 expression in R6/1 mice prevented the loss of dendritic spines in CA1 hippocampal neurons. Besides an effect on spine density, our results also suggest that genetic reduction of GRP78 may ameliorates HD hippocampal pathology by decreasing mutant huntingtin (mHtt) aggregates. Though it is not clear the mechanism, we can speculate that induction of autophagy as a result

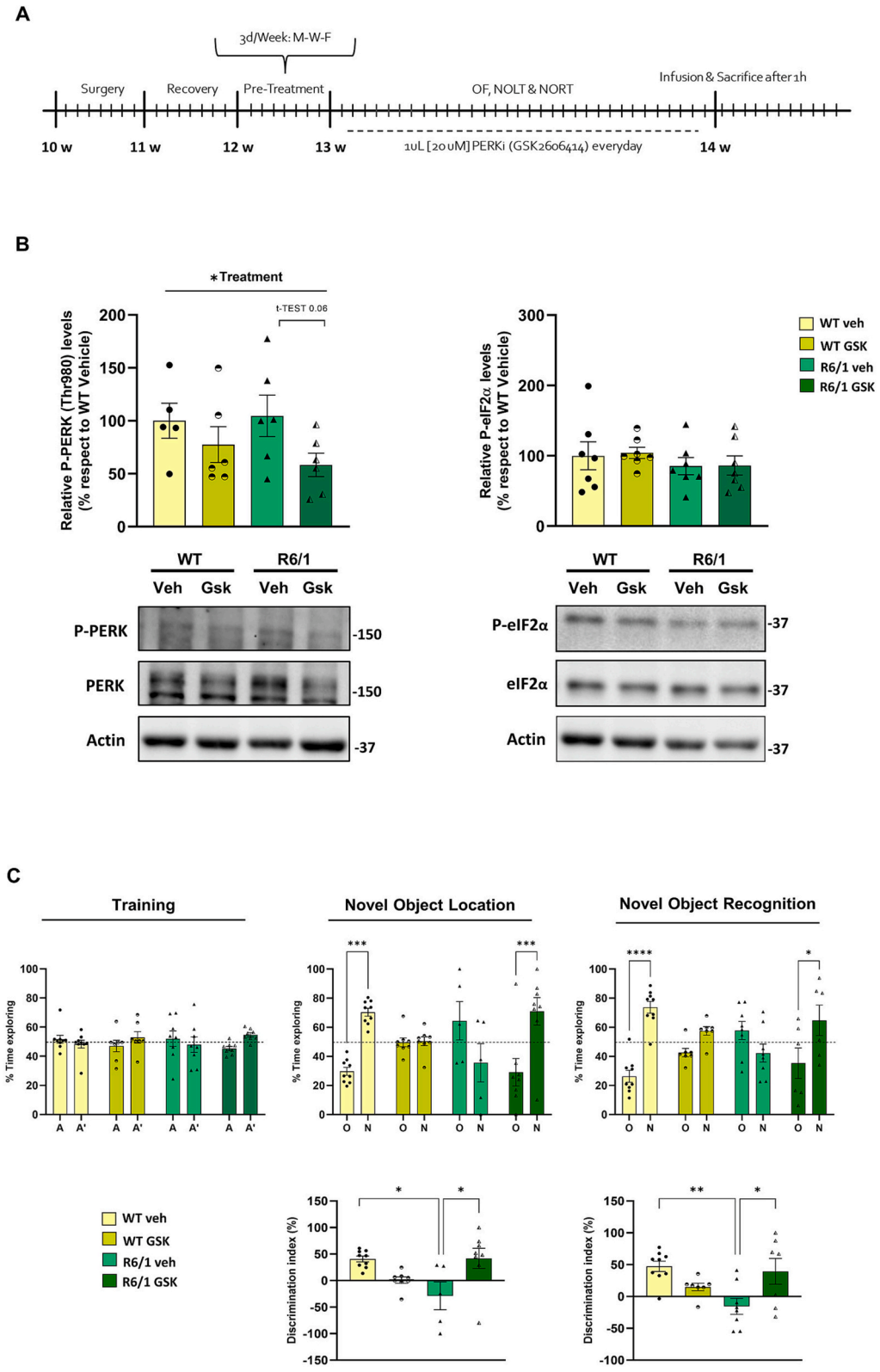

Fig. 9. PERK inhibitor GSK2606414 prevents spatial and recognition memory deficits in R6/1 mice. A Timeline representing experimental design. B Representative immunoblots showing hippocampal levels of P-PERK (Thr980), PERK, P-eIF2α (Ser 51), and eIF2α from vehicle and GSK2606414-treated mice. Actin was used as a loading control. Histograms show protein levels relative to actin and expressed as percentage of vehicle-treated WT mice. Data were analyzed by Two-way ANOVA followed by Tukey's test or *t*-Test. Data represents the mean ± SEM (n = 5–6 mice/group). C Performance in spatial and recognition memory tests. Exploration time during training and testing sessions is expressed as a percentage (%). The dashed line marks the chance level of exploration. Data were analyzed by Two-way ANOVA followed by Sídák's test. *P < 0.05, ***P < 0.001, ****P < 0.0001 compared to the percentage of time exploring the familiar object. All data represent the mean ± SEM (n = 7–9 mice/group). Discrimination indexes are expressed as a percentage (%). Data were analyzed by Two-way ANOVA followed by Tukey's test. *P < 0.05, **P < 0.01. All data represent the mean ± SEM (n = 7–9 mice/group).

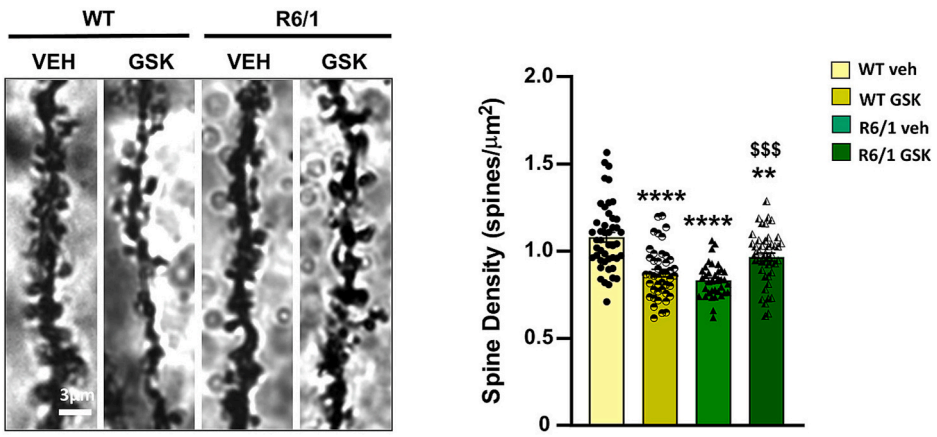

Fig. 10. PERK inhibitor GSK2606414 ameliorates hippocampal CA1 dendritic spine pathology in R6/1 mice. Representative photomicrographs showing apical dendrites from CA1 pyramidal neurons in vehicle and treated-R6/1 mice at 14 weeks of age. Scale bar 3 µm. The histogram shows a quantitative analysis of dendritic spine density per micrometer of dendritic length. Data were analyzed by Two-way ANOVA followed by Tukey's test. ****P < 0.0001 *vs* WT vehicle, $$$ P < 0.001 *vs* R6/1 vehicle. All data represent the mean ± SEM (>45 dendrites/group: n = 4 mice/group).

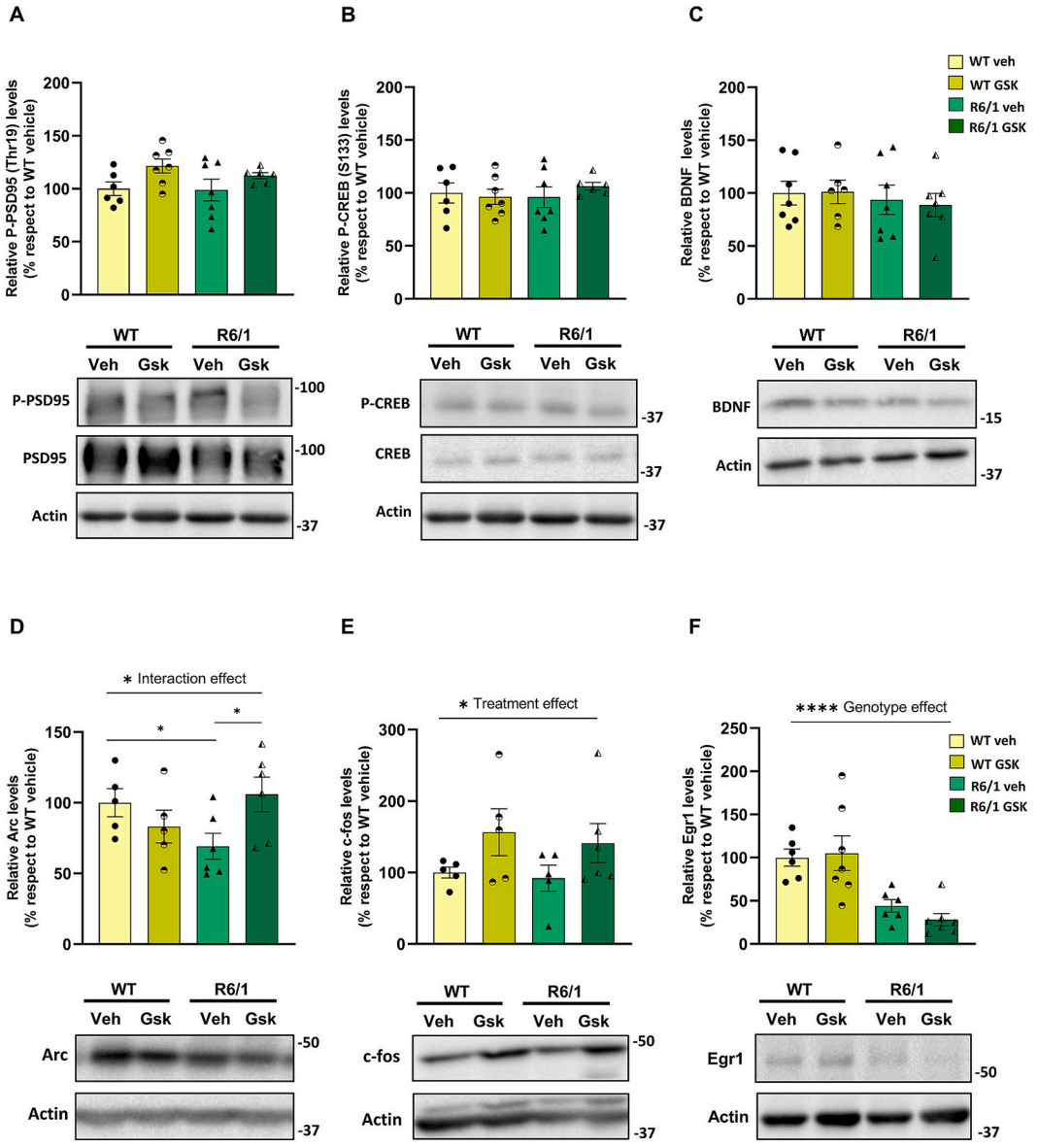

Fig. 11. PERK inhibitor GSK2606414 enhances protein levels of memory-related genes in R6/1 mice. Representative immunoblots showing P-PSD95 (Thr19), PSD95, P-CREB (Ser133), CREB, BDNF, Arc, c-fos, and Egr1 levels in total hippocampal extracts from vehicle and treated-WT and R6/1 mice at 14 weeks of age. Actin was used as a loading control. Histograms show protein levels relative to actin and expressed as percentage of WT vehicle-treated mice. Data were analyzed by Two-way ANOVA followed by Tukey's test or *t*-Test. All data represent the mean ± SEM (n = 5–6 mice/group).

of ER stress mitigation might induce degradation of mHtt aggregates. Supporting this hypothesis, it has been shown that targeting the ER stress response by knocking down XBP1, drastically reduces mHtt aggregates in HD cellular models by inducing autophagy (Vidal et al., 2012). Conversely, induction of ER stress *via* thapsigargin or tunicamycin causes aggregation of mHtt proteins through autophagy inhibition (Lee et al., 2012).

Contrary to the beneficial effect found in the hippocampus, we found that deficits in motor learning and motor coordination, behavioral tasks mostly dependent on the cortico-striatal pathway, were not prevented in R6/1 mice by reduction of GRP78. These data contrast with previous results showing that treatment of R6/2 mice with TUDCA at middle-advanced disease stages results in reduced striatal atrophy and amelioration of locomotor deficits (Keene et al., 2002). This apparent controversy may rely on the lack of an increase of GRP78 both in the striatum and cortex of R6/1 mice at early disease stages but also may reflect a different role of ER stress and in particular of GRP78 according to the HD disease stage, the brain region or even the cell population. Indeed, studies of cell type-specific transcriptomics of HD mice have revealed differential gene expression profiles across cell populations (Lee et al., 2020). In particular, in R6/2 mice has been found at early disease stages, differential expression of ER stress genes between neurons and glia or even between striatal medium spiny neurons from the direct and indirect pathways. Since our biochemistry studies do not distinguish cell populations, immunohistochemistry studies with specific neuronal and glial markers would better address this issue.

Besides the cell specific expression of GRP78 a different role of ER stress and in particular of GRP78 according to the HD disease stage or the brain region is also plausible. An example of the complexity of ER stress activation in neurodegenerative diseases is the fact that in Parkinson's Disease (PD), some authors have reported the benefits of GRP78 knockdown against the toxicity induced by α-synuclein (Salganik et al., 2015) or rotenone (Jiang et al., 2016) while others have demonstrated that upregulation of GRP78 suppresses α-synuclein aggregation and toxicity in PD rat models (Gorbatyuk et al., 2012). Therefore, even if the precise mechanisms underlying hippocampal ER stress remains unclear, to define the involvement of GRP78 activation in neuronal dysfunction and neurodegeneration in specific pathogenic conditions could be critical when designing new therapies targeting ER stress. In this scenario, the study of the UPR branches and their signaling pathways in HD may help to optimize these therapeutic interventions.

Several pieces of evidence have suggested that sustained activation of PERK impairs cognitive function due to prolonged inhibition of essential new protein synthesis involved in neuronal plasticity and memory formation (Ohno, 2018; Taalab et al., 2018). Therefore, we focused on this branch of the UPR pathways as a potential mechanism underlying hippocampal-dependent cognitive dysfunction in HD. According to the idea of a detrimental role of chronic PERK signaling in memory, the hippocampus of R6/1 mice showed increased PERK phosphorylation without any significant change in IRE1α phosphorylation or ATF6 levels. Notably, no changes in downstream effectors of these UPR sensor proteins, namely P-eIF2α and ATF4 were found pointing to a specific induction of the GRP78/PERK axis in the hippocampus of young R6/1 mice. To better clarify the role of PERK hyperactivation in HD memory alterations, GSK2606414, a well-known PERK inhibitor (Axten et al., 2012), was administered intraventricularly to R6/1 mice at the age of 12 weeks, when cognitive symptoms start to manifest. Notably, pharmacological inhibition of PERK prevented spatial and recognition memory deficits in R6/1 mice, in line with other studies showing beneficial effects of PERK inhibition in different neuropathological conditions such as AD or PD (Devi and Ohno, 2014; Ma et al., 2013; Mercado et al., 2018).

Different mechanisms may explain how PERK activation is involved in HD memory impairments. The PERK-eIF2α axis has been considered a key regulator for memory disturbances in neurodegenerative diseases and neurological conditions since phosphorylation of eIF2α inhibits general translation and stimulates ATF4 expression, repressing CREB-mediated long-term potentiation and memory (Hetz and Saxena, 2017; Hughes and Mallucci, 2019; Ohno, 2018; Zhu et al., 2016a). Thus, genetic, or pharmacological inhibition of eIF2α phosphorylation has been shown to facilitate memory (Jiang et al., 2014; Rubovitch et al., 2015). Accordingly, elevated P-eIF2α has been found in the brain of AD patients and mouse models while genetic deletion of PERK prevented synaptic plasticity and memory deficits in AD mice by reducing eIF2α phosphorylation (Ma et al., 2013). In contrast, here we have reported that inhibition of PERK is not associated with reduced phosphorylation of eIF2α even though PERK inhibition does rescue cognitive impairments in R6/1 mice. These results suggest that other molecular pathways downstream of PERK and independently of eIF2α may contribute to HD memory deficits. Actually, the prevention of spatial and recognition memory deficits in R6/1 mice treated with the PERK inhibitor was accompanied by the rescue of dendritic spine loss in CA1 pyramidal neurons suggesting that sustained PERK activation may induce a negative effect on dendritic spine formation or stability. Similar results were found in traumatic brain injury mouse models. Thus, treatment with the PERK inhibitor GSK2656157 normalized dendritic spine density in cortical neurons preventing PERK phosphorylation but not phosphorylation of eIF2α (Sen et al., 2017). Similarly, in cortical primary cultures, genetic or pharmacological inhibition of PERK rescues the loss of dendritic outgrowth reducing phosphorylation of PERK but not of eIF2α (Sen et al., 2017).

In addition, our data also point to a role of PERK phosphorylation in modulating levels of critical immediate early genes (IEGs) like Arc and c-Fos known to be rapidly and selectively upregulated underlying long-term memory (Minatohara et al., 2016). However, increased PERK phosphorylation does not affect CREB phosphorylation at Ser133 even though an association between PERK-eIF2α signaling activation and CREB dysfunction has been previously described (Costa-Mattioli et al., 2005; Devi and Ohno, 2014). In line with our results, specific knockdown of PERK in the hippocampal CA1 region of middle-aged mice enhances memory without altering P-CREB levels or other synaptic proteins such as PSD95. Although we cannot completely rule out a contribution of PERK-induced CREB dysfunction in R6/1 memory problems, other PERK-related mechanisms might be involved. Thus, it is known that PERK may contribute to the homeostasis of neuronal properties by modulating neuronal excitability, likely by regulation of neuronal calcium dynamics (Sharma et al., 2018; Zhu et al., 2016b; Zhu et al., 2016a). Since calcium dyshomeostasis can alter the activation of Ca^{+2}-dependent kinases that regulate the production of IEGs, we can hypothesize that PERK activation may contribute to memory disturbances by mechanisms related to aberrant neuronal excitability and calcium homeostasis leading to the dysregulation of synaptic proteins involved in structural and synaptic plasticity.

Overall, these data identify a novel mechanism involved in HD cognitive deficits based on the dysregulation of the GRP78/PERK axis opening a new therapeutic window in which PERK inhibition can be a beneficial treatment to prevent memory impairments in HD.

Supplementary data to this article can be found online at https://doi.org/10.1016/j.nbd.2023.106225.

Ethics approval and consent to participate

Not applicable.

Availability of data and materials

Data and material including specific experimental protocol information, are available under request.

Funding

This work was supported by the Spanish *Ministerio de Ciencia e*

Innovación (MICINN/FEDER; grants RTI2018–094374-B-I00 and PID2021-123732OB-I00 to SG, and RTI2018–095311-B-I00 to MG), *Centro de Investigación Biomédica en Red sobre Enfermedades Neurodegenerativas* (CIBERNED/ISCIII; grant PI2018/01 to SG and MG). M.E was supported by a predoctoral contract from the Spanish *Ministerio de Ciencia e Innovación (Formación de Doctores* reference PRE2019–088190), CC-I was supported by a contract from the Spanish *Ministerio de Universidades* (*Formación de Profesorado Universitario* Program, reference FPU16/02593).

Credit author statement

Silvia Gines: Conceptualization, supervision, writing original draft preparation, writing reviewing and editing. **Marc Espina**: writing original draft preparation, discussed, interpreted the data, methodology, experimental. **Nadia di Franco**: writing reviewing and editing, methodology and experimental, discussed, interpreted the data. **Martina Brañas-Navarro**: Methodology and experimental, **Irene Rodriguez Navarro**: Gene expression analysis. **Laura Lopez-Molina**: Gene expression analysis, **Veronica Brito**: Discussed, interpreted the data and provided valuable feedback. **Carlos Costas-Insua:** Writing original draft preparation, discussed, interpreted the data and provided valuable feedback. **Manuel Guzman:** Writing original draft preparation, discussed, interpreted the data and provided valuable feedback.

Declaration of Competing Interest

The authors declare no financial competing conflicts of interest in relation to this work.

Data availability

Data will be made available on request.

Acknowledgments

We are very grateful to Ana Lopez (María de Maeztu Unit of Excellence, Institute of Neurosciences, University of Barcelona, MDM-2017-0729, Ministry of Science, Innovation and Universities) and Maria Teresa Muñoz for technical assistance, Dr. Teresa Rodrigo and the staff of the animal care facility (Facultat de Psicologia Universitat de Barcelona), and Dr. Maria Calvo from the Advanced Optical Microscopy Unit from Scientific and Technological Centers from University of Barcelona for their support and advice with confocal technique.

References

Aguzzi, A., O'Connor, T., 2010. Protein aggregation diseases: pathogenicity and therapeutic perspectives. Nat. Rev. Drug Discov. 9, 237–248. https://doi.org/10.1038/nrd3050.

Anglada-Huguet, M., Xifró, X., Giralt, A., Zamora-Moratalla, A., Martín, E.D., Alberch, J., 2014. Prostaglandin E2 EP1 receptor antagonist improves motor deficits and rescues memory decline in R6/1 mouse model of Huntington's disease. Mol. Neurobiol. 49, 784–795. https://doi.org/10.1007/s12035-013-8556-x.

Axten, J.M., Medina, J.R., Feng, Y., Shu, A., Romeril, S.P., Grant, S.W., Li, W.H.H., Heerding, D.A., Minthorn, E., Mencken, T., Atkins, C., Liu, Q., Rabindran, S., Kumar, R., Hong, X., Goetz, A., Stanley, T., Taylor, J.D., Sigethy, S.D., Tomberlin, G. H., Hassell, A.M., Kahler, K.M., Shewchuk, L.M., Gampe, R.T., 2012. Discovery of 7-methyl-5-(1-{[3-(trifluoromethyl)phenyl]acetyl}-2,3-dihydro- 1H-indol-5-yl)-7H-pyrrolo[2,3-d]pyrimidin-4-amine (GSK2606414), a potent and selective first-in-class inhibitor of protein kinase R (PKR)-like endoplasmic reticulum kinase (PERK). J. Med. Chem. 55, 7193–7207. https://doi.org/10.1021/jm300713s.

Bates, G., 2003. Huntingtin aggregation and toxicity in Huntington's disease. Lancet 361, 1642–1644. https://doi.org/10.1016/S0140-6736(03)13304-1.

Begeti, F., Schwab, L.C., Mason, S.L., Barker, R.A., 2016. Hippocampal dysfunction defines disease onset in Huntington's disease. J. Neurol. Neurosurg. Psychiatry 87, 975–981. https://doi.org/10.1136/jnnp-2015-312413.

Bertram, L., Tanzi, R.E., 2005. The genetic epidemiology of neurodegenerative disease. J. Clin. Investig. 115, 1449–1457. https://doi.org/10.1172/JCI24761.

Brito, V., Giralt, A., Enriquez-Barreto, L., Puigdellívol, M., Suelves, N., Zamora-moratalla, A., Ballesteros, J.J., Martín, E.D., Dominguez-iturza, N., Morales, M., Alberch, J., Ginés, S., 2014. Neurotrophin receptor p75 NTR mediates Huntington's disease – associated synaptic and memory dysfunction. J. Clin. Invest. 124, 4411–4428. https://doi.org/10.1172/JCI74809.long-term.

Cai, F., Liu, J., Li, C., Wang, J., 2015. Critical role of endoplasmic reticulum stress in cognitive impairment induced by microcystin-LR. Int. J. Mol. Sci. 16, 28077–28086. https://doi.org/10.3390/ijms161226083.

Cai, M., Hu, J. Yun, Liu, B., Bei, Li, Jing, J., Li, F., Lou, S., 2020. The molecular mechanisms of excessive hippocampal endoplasmic reticulum stress depressing cognition-related proteins expression and the regulatory effects of Nrf2. Neuroscience 431, 152–165. https://doi.org/10.1016/j.neuroscience.2020.02.001.

Carnemolla, A., Fossale, E., Agostoni, E., Michelazzi, S., Calligaris, R., de Maso, L., del Sal, G., MacDonald, M.E., Persichetti, F., 2009. Rrs1 is involved in endoplasmic reticulum stress response in Huntington disease. J. Biol. Chem. 284, 18167–18173. https://doi.org/10.1074/jbc.M109.018325.

Casas, C., 2017. GRP78 at the Centre of the stage in cancer and neuroprotection. Front. Neurosci. 11, 1–15. https://doi.org/10.3389/fnins.2017.00177.

Costa-Mattioli, M., Gobert, D., Harding, H., Herdy, B., Azzi, M., Bruno, M., Bidinosti, M., Ben Mamou, C., Marcinkiewicz, E., Yoshida, M., Imataka, H., Cuello, A.C., Seidah, N., Sossin, W., Lacaille, J.C., Ron, D., Nader, K., Sonenberg, N., 2005. Translational control of hippocampal synaptic plasticity and memory by the eIF2α kinase GCN2. Nature 436, 1166–1170. https://doi.org/10.1038/nature03897.

Devi, L., Ohno, M., 2014. PERK mediates eIF2α phosphorylation responsible for BACE1 elevation, CREB dysfunction and neurodegeneration in a mouse model of Alzheimer's disease. Neurobiol. Aging 35, 2272–2281. https://doi.org/10.1016/j.neurobiolaging.2014.04.031.

DiFiglia, M., Sapp, E., Chase, K.O., Davies, S.W., Bates, G.P., Vonsattel, J.P., Aronin, N., 1997. Aggregation of huntingtin in neuronal intranuclear inclusions and dystrophic neurites in brain. Science 1979 (277), 1990–1993. https://doi.org/10.1126/science.277.5334.1990.

Duennwald, M.L., Lindquist, S., 2008. Impaired ERAD and ER stress are early and specific events in polyglutamine toxicity. Genes Dev. 22, 3308–3319. https://doi.org/10.1101/gad.1673408.

Fernandez-Fernandez, M.R., Ferrer, I., Lucas, J.J., 2011. Impaired ATF6α processing, decreased Rheb and neuronal cell cycle re-entry in Huntington's disease. Neurobiol. Dis. 41, 23–32. https://doi.org/10.1016/j.nbd.2010.08.014.

García-Forn, M., Martínez-Torres, S., García-Díaz Barriga, G., Alberch, J., Milà, M., Azkona, G., Pérez-Navarro, E., 2018. Pharmacogenetic modulation of STEP improves motor and cognitive function in a mouse model of Huntington's disease. Neurobiol. Dis. 120, 88–97. https://doi.org/10.1016/j.nbd.2018.08.024.

Giralt, A., Saavedra, A., Alberch, J., Pérez-Navarro, E., 2012. Cognitive dysfunction in Huntington's disease: humans, mouse models and molecular mechanisms. J Huntingtons Dis. https://doi.org/10.3233/JHD-120023.

Giralt, A., Saavedra, A., Carretón, O., Arumí, H., Tyebji, S., Alberch, J., Pérez-Navarro, E., 2013. PDE10 inhibition increases GluA1 and CREB phosphorylation and improves spatial and recognition memories in a Huntington's disease mouse model. Hippocampus 23, 684–695. https://doi.org/10.1002/hipo.22128.

Gorbatyuk, M.S., Shabashvili, A., Chen, W., Meyers, C., Sullivan, L.F., Salganik, M., Lin, J.H., Lewin, A.S., Muzyczka, N., Gorbatyuk, O.S., 2012. Glucose regulated protein 78 diminishes α-synuclein neurotoxicity in a rat model of parkinson disease. Mol. Ther. 20, 1327–1337. https://doi.org/10.1038/mt.2012.28.

Gupta, P., Tiwari, S., Singh, A., Pal, A., Mishra, A., Singh, S., 2021. Rivastigmine attenuates the Alzheimer's disease related protein degradation and apoptotic neuronal death signalling. Biochem. J. 478, 1435–1451. https://doi.org/10.1042/BCJ20200754.

Han, J., Back, S., Hur, J., Lin, Y.-H., Gildersleeve, R., Shan, J., Yuan, C.L., Krokowski, D., Wang, S., Hatzoglou, M., Kilberg, M.S., Sartor, M.A., Kaufman, R.J., 2013. ER-stress-induced transcriptional regulation increases protein synthesis leading to cell death. Nat. Cell Biol. 15, 481–490. https://doi.org/10.1038/ncb2738.

Harris, K.L., Armstrong, M., Swain, R., Erzinclioglu, S., Das, T., Burgess, N., Barker, R.A., Mason, S.L., 2019. Huntington's disease patients display progressive deficits in hippocampal-dependent cognition during a task of spatial memory. Cortex 119, 417–427. https://doi.org/10.1016/j.cortex.2019.07.014.

Herdegen, T., Leah, J.D., 1998. Inducible and constitutive transcription factors in the mammalian nervous system: control of gene expression by Jun, Fos and Krox, and CREB/ATF proteins. Brain Res. Rev. https://doi.org/10.1016/S0165-0173(98)00018-6.

Hetz, C., Papa, F.R., 2018. The unfolded protein response and cell fate control. Mol. Cell 69, 169–181. https://doi.org/10.1016/j.molcel.2017.06.017.

Hetz, C., Saxena, S., 2017. ER stress and the unfolded protein response in neurodegeneration. Nat. Rev. Neurol. 13, 477–491. https://doi.org/10.1038/nrneurol.2017.99.

Hetz, C., Chevet, E., Oakes, S.A., 2015. Proteostasis control by the unfolded protein response. Nat. Cell Biol. https://doi.org/10.1038/ncb3184.

Hughes, D., Mallucci, G.R., 2019. The unfolded protein response in neurodegenerative disorders – therapeutic modulation of the PERK pathway. FEBS J. https://doi.org/10.1111/febs.14422.

Jiang, H.Q., Ren, M., Jiang, H.Z., Wang, J., Zhang, J., Yin, X., Wang, S.Y., Qi, Y., Wang, X.D., Feng, H.L., 2014. Guanabenz delays the onset of disease symptoms, extends lifespan, improves motor performance and attenuates motor neuron loss in the SOD1 G93A mouse model of amyotrophic lateral sclerosis. Neuroscience 277, 132–138. https://doi.org/10.1016/j.neuroscience.2014.03.047.

Jiang, M., Yun, Q., Shi, F., Niu, G., Gao, Y., Xie, S., Yu, S., 2016. Downregulation of miR-384-5p attenuates rotenone-induced neurotoxicity in dopaminergic SH-SY5Y cells through inhibiting endoplasmic reticulum stress. Am. J. Phys. Cell Phys. 310, C755–C763. https://doi.org/10.1152/ajpcell.00226.2015.

Keene, C.D., Rodrigues, C.M.P., Eich, T., Chhabra, M.S., Steer, C.J., Low, W.C., 2002. Tauroursodeoxycholic acid, a bile acid, is neuroprotective in a transgenic animal

model of Huntington's disease. Proc. Natl. Acad. Sci. U. S. A. 99, 10671–10676. https://doi.org/10.1073/pnas.162362299.
Keshk, W.A., Elseady, W.S., Sarhan, N.I., Zineldeen, D.H., 2020. Curcumin attenuates cytoplasmic/endoplasmic reticulum stress, apoptosis and cholinergic dysfunction in diabetic rat hippocampus. Metab. Brain Dis. 35, 637–647. https://doi.org/10.1007/s11011-020-00551-0.
Korb, E., Finkbeiner, S., 2011. Arc in synaptic plasticity: from gene to behavior. Trends Neurosci. https://doi.org/10.1016/j.tins.2011.08.007.
Kou, J., Wang, M., Shi, J., Zhang, H., Pu, X., Song, S., Yang, C., Yan, Y., Döring, Y., Xie, X., Pang, X., 2021. Curcumin reduces cognitive deficits by inhibiting Neuroinflammation through the endoplasmic reticulum stress pathway in apolipoprotein E4 transgenic mice. ACS Omega 6, 6654–6662. https://doi.org/10.1021/acsomega.0c04810.
Langfelder, P., Cantle, J.P., Chatzopoulou, D., Wang, N., Gao, F., Al-Ramahi, I., Lu, X.H., Ramos, E.M., El-Zein, K., Zhao, Y., Deverasetty, S., Tebbe, A., Schaab, C., Lavery, D. J., Howland, D., Kwak, S., Botas, J., Aaronson, J.S., Rosinski, J., Coppola, G., Horvath, S., Yang, X.W., 2016 Apr. Integrated genomics and proteomics define huntingtin CAG length-dependent networks in mice. Nat. Neurosci. 19 (4), 623–633. https://doi.org/10.1038/nn.4256.
Lee, H., Fenster, R.J., Pineda, S.S., Gibbs, W.S., Mohammadi, S., Davila-Velderrain, J., Garcia, F.J., Therrien, M., Novis, H.S., Gao, F., Wilkinson, H., Vogt, T., Kellis, M., LaVoie, M.J., Heiman, M., 2020. Cell Type-Specific Transcriptomics Reveals that Mutant Huntingtin Leads to Mitochondrial RNA Release and Neuronal Innate Immune Activation. Neuron 107 (5), 891–908. e8. https://doi.org/10.1016/j.neuron.2020.06.021.
Lee, H., Noh, J.Y., Oh, Y., Kim, Y., Chang, J.W., Chung, C.W., Lee, S.T., Kim, M., Ryu, H., Jung, Y.K., 2012. IRE1 plays an essential role in ER stress-mediated aggregation of mutant huntingtin via the inhibition of autophagy flux. Hum. Mol. Genet. 21, 101–114. https://doi.org/10.1093/hmg/ddr445.
Leitman, J., Ulrich Hartl, F., Lederkremer, G.Z., 2013. Soluble forms of polyQ-expanded huntingtin rather than large aggregates cause endoplasmic reticulum stress. Nat. Commun. 4 https://doi.org/10.1038/NCOMMS3753.
Leitman, J., Barak, B., Benyair, R., Shenkman, M., Ashery, U., Hartl, F.U., Lederkremer, G.Z., 2014. ER stress-induced eIF2-alpha phosphorylation underlies sensitivity of striatal neurons to pathogenic huntingtin. PLoS One 9. https://doi.org/10.1371/journal.pone.0090803.
Li, F., Liu, B. Bei, Cai, M., Li, J., Jing, Lou, Jie, S., 2018. Excessive endoplasmic reticulum stress and decreased neuroplasticity-associated proteins in prefrontal cortex of obese rats and the regulatory effects of aerobic exercise. Brain Res. Bull. 140, 52–59. https://doi.org/10.1016/j.brainresbull.2018.04.003.
Lin, L., Cao, J., Yang, S.S., Fu, Z.Q., Zeng, P., Chu, J., Ning, L.N., Zhang, T., Shi, Y., Tian, Q., Zhou, X.W., Wang, J.Z., 2018. Endoplasmic reticulum stress induces spatial memory deficits by activating GSK-3. J. Cell. Mol. Med. 22, 3489–3502. https://doi.org/10.1111/jcmm.13626.
Liu, D.C., Eagleman, D.E., Tsai, N.P., 2019. Novel roles of ER stress in repressing neural activity and seizures through Mdm2- and p53-dependent protein translation. PLoS Genet. 15 (9), e1008364 https://doi.org/10.1371/journal.pgen.1008364.
Liu, D.C., Lee, K.Y., Lizarazo, S., Cook, J.K., Tsai, N.P., 2021. ER stress-induced modulation of neural activity and seizure susceptibility is impaired in a fragile X syndrome mouse model. Neurobiol. Dis. 158, 105450 https://doi.org/10.1016/j.nbd.2021.105450.
Luo, S., Mao, C., Lee, B., Lee, A.S., 2006. GRP78/BiP is required for cell proliferation and protecting the inner cell mass from apoptosis during early mouse embryonic development. Mol. Cell. Biol. 26, 5688–5697. https://doi.org/10.1128/mcb.00779-06.
Ma, T., Trinh, M.A., Wexler, A.J., Bourbon, C., Gatti, E., Pierre, P., Cavener, D.R., Klann, E., 2013. Suppression of eIF2α kinases alleviates Alzheimer's disease-related plasticity and memory deficits. Nat. Neurosci. 16, 1299–1305. https://doi.org/10.1038/nn.3486.
Mangiarini, L., Sathasivam, K., Seller, M., Cozens, B., Harper, A., Hetherington, C., Lawton, M., Trottier, Y., Lehrach, H., Davies, S.W., Bates, G.P., 1996. Exon I of the HD gene with an expanded CAG repeat is sufficient to cause a progressive neurological phenotype in transgenic mice. Cell 87, 493–506. https://doi.org/10.1016/S0092-8674(00)81369-0.
Matthias, E., Ravi Kiran Reddy, K., Joaquin, G.L., Susana, M., Kameshwar, R.S., 2015. The unfolded protein response and its potential role in Huntington's disease elucidated by a systems biology approach. F1000Res 4. https://doi.org/10.12688/f1000research.6358.2.
Mercado, G., Castillo, V., Soto, P., López, N., Axten, J.M., Sardi, S.P., Hoozemans, J.J.M., Hetz, C., 2018. Targeting PERK signaling with the small molecule GSK2606414 prevents neurodegeneration in a model of Parkinson's disease. Neurobiol. Dis. 112, 136–148. https://doi.org/10.1016/j.nbd.2018.01.004.
Minatohara, K., Akiyoshi, M., Okuno, H., 2016. Role of immediate-early genes in synaptic plasticity and neuronal ensembles underlying the memory trace. Front. Mol. Neurosci. 8, 78. https://doi.org/10.3389/FNMOL.2015.00078/BIBTEX.
Moreno, J.A., Radford, H., Peretti, D., Steinert, J.R., Verity, N., Martin, M.G., Halliday, M., Morgan, J., Dinsdale, D., Ortori, C.A., Barrett, D.A., Tsaytler, P., Bertolotti, A., Willis, A.E., Bushell, M., Mallucci, G.R., 2012. Sustained translational repression by eIF2α-P mediates prion neurodegeneration. Nature 485, 507–511. https://doi.org/10.1038/nature11058.
Moreno, J.A., Halliday, M., Molloy, C., Radford, H., Verity, N., Axten, J.M., Ortori, C.A., Willis, A.E., Fischer, P.M., Barrett, D.A., Mallucci, G.R., 2013. Oral treatment targeting the unfolded protein response prevents neurodegeneration and clinical disease in prion-infected mice. Sci. Transl. Med. 5 https://doi.org/10.1126/scitranslmed.3006767.
Ohno, M., 2018. PERK as a hub of multiple pathogenic pathways leading to memory deficits and neurodegeneration in Alzheimer's disease. Brain Res. Bull. 141, 72–78. https://doi.org/10.1016/j.brainresbull.2017.08.007.
Puigdellívol, M., Cherubini, M., Brito, V., Giralt, A., Suelves, N., Ballesteros, J., Zamora-Moratalla, A., Martín, E.D., Eipper, B.A., Alberch, J., Ginés, S., 2015. A role for Kalirin-7 in corticostriatal synaptic dysfunction in Huntington's disease. Hum. Mol. Genet. 7265–85 https://doi.org/10.1093/hmg/ddv426.
Puigdellívol, M., Saavedra, A., Pérez-Navarro, E., 2016. Cognitive dysfunction in Huntington's disease: mechanisms and therapeutic strategies beyond BDNF. Brain Pathol. 26, 752–771. https://doi.org/10.1111/bpa.12432.
Radford, H., Moreno, J.A., Verity, N., Halliday, M., Mallucci, G.R., 2015. PERK inhibition prevents tau-mediated neurodegeneration in a mouse model of frontotemporal dementia. Acta Neuropathol. 130, 633–642. https://doi.org/10.1007/s00401-015-1487-z.
Ramalho, R.M., Nunes, A.F., Dias, R.B., Amaral, J.D., Lo, A.C., D'Hooge, R., Sebastião, A. M., Rodrigues, C.M.P., 2013. Tauroursodeoxycholic acid suppresses amyloid β-induced synaptic toxicity in vitro and in APP/PS1 mice. Neurobiol. Aging 34, 551–561. https://doi.org/10.1016/j.neurobiolaging.2012.04.018.
Reijonen, S., Putkonen, N., Nørremølle, A., Lindholm, D., Korhonen, L., 2008. Inhibition of endoplasmic reticulum stress counteracts neuronal cell death and protein aggregation caused by N-terminal mutant huntingtin proteins. Exp. Cell Res. 314, 950–960. https://doi.org/10.1016/j.yexcr.2007.12.025.
Riccardi, W.X., Wolfner, D.F., Clark, M.F., 2015. The genetic architecture of the genome-wide transcriptional response to ER stress in the mouse. PLoS Genet. 11, 1004924. https://doi.org/10.1371/journal.pgen.1004924.
Rubovitch, V., Barak, S., Rachmany, L., Goldstein, R.B., Zilberstein, Y., Pick, C.G., 2015. The neuroprotective effect of Salubrinal in a mouse model of traumatic brain injury. NeuroMolecular Med. 17, 58–70. https://doi.org/10.1007/s12017-015-8340-3.
Salganik, M., Sergeyev, V.G., Shinde, V., Meyers, C.A., Gorbatyuk, M.S., Lin, J.H., Zolotukhin, S., Gorbatyuk, O.S., 2015. The loss of glucose-regulated protein 78 (GRP78) during normal aging or from siRNA knockdown augments human alpha-synuclein (α-syn) toxicity to rat nigral neurons. Neurobiol. Aging 36, 2213–2223. https://doi.org/10.1016/j.neurobiolaging.2015.02.018.
Sen, N., 2019. ER stress, CREB, and memory: a tangled emerging link in disease. Neuroscientist. https://doi.org/10.1177/1073858418816611.
Sen, T., Gupta, R., Kaiser, H., Sen, N., 2017. Activation of PERK elicits memory impairment through inactivation of CREB and downregulation of PSD95 after traumatic brain injury. J. Neurosci. 37, 5900–5911. https://doi.org/10.1523/JNEUROSCI.2343-16.2017.
Shacham, T., Sharma, N., Lederkremer, G.Z., 2019. Protein misfolding and ER stress in Huntington's disease. Front. Mol. Biosci. 6 https://doi.org/10.3389/fmolb.2019.00020.
Shacham, T., Patel, C., Lederkremer, G.Z., 2021. Perk pathway and neurodegenerative disease: to inhibit or to activate? Biomolecules 11, 1–21. https://doi.org/10.3390/biom11030354.
Sharma, V., Ounallah-Saad, H., Chakraborty, D., Hleihil, M., Sood, R., Barrera, I., Edry, E., Chandran, S.K., de Leon, S.B.T., Kaphzan, H., Rosenblum, K., 2018. Local inhibition of PERK enhances memory and reverses age-related deterioration of cognitive and neuronal properties. J. Neurosci. 38, 648–658. https://doi.org/10.1523/JNEUROSCI.0628-17.2017.
Soto, C., 2003. Unfolding the role of protein misfolding in neurodegenerative diseases. Nat. Rev. Neurosci. 4, 49–60. https://doi.org/10.1038/nrn1007.
Spires, T.L., Grote, H.E., Garry, S., Cordery, P.M., Van Dellen, A., Blakemore, C., Hannan, A.J., 2004. Dendritic spine pathology and deficits in experience-dependent dendritic plasticity in R6/1 Huntington's disease transgenic mice. Eur. J. Neurosci. 19, 2799–2807. https://doi.org/10.1111/j.0953-816X.2004.03374.x.
Taalab, Y.M., Ibrahim, N., Maher, A., Hassan, M., Mohamed, W., Moustafa, A.A., Salama, M., Johar, D., Bernstein, L., 2018. Mechanisms of disordered neurodegenerative function: concepts and facts about the different roles of the protein kinase RNA-like endoplasmic reticulum kinase (PERK). Rev. Neurosci. 29, 387–415. https://doi.org/10.1515/revneuro-2017-0071.
Tabas, I., Ron, D., 2011. Integrating the mechanisms of apoptosis induced by endoplasmic reticulum stress. Nat. Cell Biol. 13, 184–190. https://doi.org/10.1038/ncb0311-184.
Urra, H., Dufey, E., Lisbona, F., Rojas-Rivera, D., Hetz, C., 2013. When ER stress reaches a dead end. Biochim. Biophys. Acta, Mol. Cell Res. 1833, 3507–3517. https://doi.org/10.1016/j.bbamcr.2013.07.024.
Vidal, R.L., Figueroa, A., Court, F.A., Thielen, P., Molina, C., Wirth, C., Caballero, B., Kiffin, R., Segura-Aguilar, J., Cuervo, A.M., Glimcher, L.H., Hetz, C., 2012. Targeting the UPR transcription factor XBP1 protects against Huntington's disease through the regulation of FoxO1 and autophagy. Hum. Mol. Genet. 21 (10), 2245–2262. https://doi.org/10.1093/hmg/dds040.
Vonsattel, J.P., Myers, R.H., Stevens, T.J., Ferrante, R.J., Bird, E.D., Richardson, E.P., 1985. Neuropathological classification of huntington's disease. J. Neuropathol. Exp. Neurol. 44, 559–577. https://doi.org/10.1097/00005072-198511000-00003.
Walter, P., Ron, D., 2011. The unfolded protein response: from stress pathway to homeostatic regulation. Science 1979. https://doi.org/10.1126/science.1209038.
Wang, M., Wey, S., Zhang, Y., Ye, R., Lee, A.S., 2009. Role of the unfolded protein response regulator GRP78/BiP in development, cancer, and neurological disorders. Antioxid. Redox Signal. 11, 2307–2316. https://doi.org/10.1089/ars.2009.2485.
Xu, F., Zhang, G., Yin, J., Zhang, Q., Ge, M., Peng, L., Wang, S., Li, Y., 2019. Fluoxetine mitigating late-stage cognition and neurobehavior impairment induced by cerebral ischemia reperfusion injury through inhibiting ERS-mediated neurons apoptosis in the hippocampus. Behav. Brain Res. 370, 111952. https://doi.org/10.1016/j.bbr.2019.111952.

Yan, F., Cao, S., Li, J., Dixon, B., Yu, X., Chen, J., Gu, C., Lin, W., Chen, G., 2017. Pharmacological inhibition of PERK attenuates early brain injury after subarachnoid hemorrhage in rats through the activation of Akt. Mol. Neurobiol. 54, 1808–1817. https://doi.org/10.1007/s12035-016-9790-9.

Zhu, S., Henninger, K., McGrath, B.C., Cavener, D.R., 2016a. PERK regulates working memory and protein synthesis-dependent memory flexibility. PLoS One 11, 1–15. https://doi.org/10.1371/journal.pone.0162766.

Zhu, S., McGrath, B.C., Bai, Y., Tang, X., Cavener, D.R., 2016b. PERK regulates Gq protein-coupled intracellular Ca2+ dynamics in primary cortical neurons. Mol Brain 9, 1–11. https://doi.org/10.1186/s13041-016-0268-5.